

A STUDY ON INTEGRAL RECYCLING OF VALUABLE PARTICLE
EMBEDDED COMPOSITE WASTES

A THESIS SUBMITTED TO
THE GRADUATE SCHOOL OF NATURAL AND APPLIED SCIENCES
OF
MIDDLE EAST TECHNICAL UNIVERSITY

BY

TANSU GÖYNÜK

IN PARTIAL FULFILLMENT OF THE REQUIREMENTS
FOR
THE DEGREE OF MASTER OF SCIENCE
IN
METALLURGICAL AND MATERIALS ENGINEERING

JANUARY 2019

Approval of the thesis:

**A STUDY ON INTEGRAL RECYCLING OF VALUABLE PARTICLE
EMBEDDED COMPOSITE WASTES**

submitted by **TANSU GÖYNÜK** in partial fulfillment of the requirements for the degree of **Master of Science in Metallurgical and Materials Engineering Department, Middle East Technical University** by,

Prof. Dr. Halil Kalıpçılar
Dean, Graduate School of **Natural and Applied Sciences**

Prof. Dr. Cemil Hakan Gür
Head of Department, **Met. and Mat. Eng.**

Prof. Dr. İshak Karakaya
Supervisor, **Met. and Mat. Eng., METU**

Examining Committee Members:

Prof. Dr. Kadri Aydınol
Met. and Mat. Eng., METU

Prof. Dr. İshak Karakaya
Met. and Mat. Eng., METU

Assist. Prof. Dr. Batur Ercan
Met. and Mat. Eng., METU

Assist. Prof. Dr. Metehan Erdoğan
Met. and Mat. Eng., Yıldırım Beyazıt Uni.

Assist. Prof. Dr. Erkan Konca
Met. and Mat. Eng., Atılım Uni.

Date: 21.01.2019

I hereby declare that all information in this document has been obtained and presented in accordance with academic rules and ethical conduct. I also declare that, as required by these rules and conduct, I have fully cited and referenced all material and results that are not original to this work.

Name, Surname: Tansu Göynük

Signature:

ABSTRACT

A STUDY ON INTEGRAL RECYCLING OF VALUABLE PARTICLE EMBEDDED COMPOSITE WASTES

Göynük, Tansu
Master of Science, Metallurgical and Materials Engineering
Supervisor: Prof. Dr. İshak Karakaya

January 2019, 75 pages

Recovery of the valuable particle embedded composite cutting tools was achieved by electrodisolution and deposition techniques. Diamond embedded composite wastes including both bronze matrix and cobalt-copper-tin matrix were used to recycle comprehensively and efficiently within the scope of this thesis. The parameters like current density, temperature and electrolyte composition were optimized to obtain both diamond and metal constituents as compact, dense powder with minimum specific surface area and average particle size. Scanning electron microscope images, X-Ray diffraction analysis, particle size measurements and specific surface area measurements were evaluated to understand the effects of parameters on the electrodeposited powder qualities.

Effects of hydrogen evolution on the properties of the collected metal powders were observed during optimization of the electrodeposition conditions. The morphology and the orientation of the powder growth were found to be affected by the hydrogen evolution reaction.

Keywords: Diamond Recycling, Cutting Tool Recycling, Galvanostatic Electrodeposition, Powder Formation

ÖZ

DEĞERLİ PARÇACIK GÖMÜLÜ KOMPOZİT ATIKLARIN ENTEGRE GERİ DÖNÜŞÜMÜ

Göynük, Tansu
Yüksek Lisans, Metalurji ve Malzeme Mühendisliği
Tez Danışmanı: Prof. Dr. İshak Karakaya

Ocak 2019, 75 sayfa

Elektro-çözündürme ve elektro-biriktirme teknikleri kullanılarak değerli parçacık gömülü kompozit kesici uçların geri dönüşümü gerçekleştirildi. Bu tez kapsamında pirinç ve kobalt-bakır-kalay içerikli iki farklı matrisli elmas gömülü kompozit atıklar kapsamlı ve etkin geri dönüşüm için anot olarak kullanıldı. Atık kesici uçların içeriğindeki elmasın ve minimum özgül yüzey alanı ve ortalama tane boyutuna sahip kompakt, yoğun metal bileşenlerin toz olarak elde edilebilmesi için akım yoğunluğu, sıcaklık ve elektrolit kompozisyonu gibi parametreler optimize edildi. Parametrelerin elektro-biriktirilmiş tozların üzerindeki etkisini inceleyebilmek için taramalı elektron mikroskobu görüntüleri, X ışını kırınım analizleri, toz boyutu ölçümleri ve özgül yüzey alanı ölçümleri yapıldı.

Elektro-biriktirme koşullarının optimizasyonu sırasında hidrojen oluşum reaksiyonunun elektro-biriktirilmiş metal tozları üzerindeki etkisi de gözlemlenmiştir. Elektrokimyasal yöntemle toplanan tozların morfolojisi ve tozların büyüme yönünün hidrojen oluşum reaksiyonu ile etkilendiği sonucu elde edildi.

Anahtar Kelimeler: Elmas Geri Dönüşümü, Kesici Uçların Geri Dönüşümü,
Galvanostatik Elektrodepozisyon, Toz Oluşturma

To my family

ACKNOWLEDGMENTS

I would like to express my deepest gratitude to my advisor Prof. Dr. İshak Karakaya for the guidance and the encouragement during my graduate studying period through his experience, knowledge, patience, support, motivation and enthusiasm. I also want to show my appreciation to Assist. Prof. Dr. Metehan Erdoğan for guidance and support.

My special thanks go to my love Burak Göynük for his friendship, encouragements, support, help and apprehension throughout my life.

Moreover, I would like to thank the Scientific Research Projects (BAP) with project number of GAP-308-2018-2681 of Middle East Technical University and the Scientific and Technological Research Council of Türkiye (TÜBİTAK) through the project 116M406.

I am grateful to my chance angels Sedanur Toraman and Hilal Kılınç Seyhun for their moral support and friendship. Although I had a hard time due to various reasons, they always stood beside me and encouraged me. I would like to extend my gratitude to my lab mates for their support, help and friendship during thesis study.

Furthermore, I am indebted to my colleague Mertcan Başkan not only his academic support but also for his friendship, understanding and endless motivation in my life. Additionally, thanks to my leader Orkun Umur Önem who always approached me with patience and love.

Finally, I thank my family for their endless support and love. I would like to give the unlimited gratitude and appreciation to my father, mother, sister, father-in-law, mother-in-law and sister-in-law.

TABLE OF CONTENTS

| | |
|---|------|
| ABSTRACT | v |
| ÖZ | vii |
| ACKNOWLEDGMENTS | x |
| TABLE OF CONTENTS | xi |
| LIST OF TABLES | xiii |
| LIST OF FIGURES | xiv |
| 1. INTRODUCTION | 1 |
| 1.1. The Purpose of the Thesis | 6 |
| 2. LITERATURE REVIEW | 9 |
| 2.1. Electrodeposition of Metallic Powders | 9 |
| 2.1.1. Potentiostatic and Galvanostatic Powder Electrodeposition | 9 |
| 2.1.2. Surface Area of Electrodeposited Metal Powders | 14 |
| 2.1.3. Particle Size and Apparent Density of Electrodeposited Metal Powders | 16 |
| 2.1.4. Hydrogen Co-Deposition | 17 |
| 2.2. Cutting Tools and Importance of Cutting Tools Materials Recycling | 17 |
| 2.3. Current Methods of Recovering Valuable Particle Embedded Cutting Tools | 18 |
| 3. EXPERIMENTAL | 21 |
| 3.1. Electrolytic Cell | 21 |
| 3.2. Recycling of Diamond Embedded Copper-Tin Matrix Cutting Tools | 23 |
| 3.3. Recycling of Diamond Embedded Cobalt-Copper-Tin Matrix Cutting Tools | 25 |
| 3.4. Characterization of Collected Powders | 28 |
| 4. RESULTS | 29 |

| | |
|--|----|
| 4.1. Recovery of Diamond Particles from Metal Matrix Composite Cutting Tools | 29 |
| 4.2. Recovery of Metals from Cu-Sn Matrix Composite Cutting Tools..... | 30 |
| 4.2.1. Tin Powders..... | 30 |
| 4.3. Specific Surface Area of Electrodeposited Copper Powder | 30 |
| 4.4. Particle Size of Electrodeposited Copper Powder | 37 |
| 4.5. Specific Surface Area and Particle Size of Cobalt-Copper-Tin Powder | 39 |
| 5. DISCUSSION | 43 |
| 5.1. Diamond Embedded Copper-Tin Matrix Cutting Tools | 43 |
| 5.1.1. Morphology of Electrodeposited Copper Powders | 43 |
| 5.1.1.1. Effect of Current Density..... | 43 |
| 5.1.1.2. Effect of Temperature..... | 46 |
| 5.1.1.3. Effect of Electrolyte Composition | 48 |
| 5.1.2. Crystallography of Electrodeposited Copper Powders | 52 |
| 5.2. Diamond Embedded Cobalt-Copper-Tin Matrix Cutting Tools | 56 |
| 5.2.1. Morphology of the Electrodeposited Cobalt-Copper-Tin Powders | 56 |
| 5.2.1.1. Effect of Current Density..... | 57 |
| 5.2.1.2. Effect of Temperature..... | 60 |
| 5.2.1.3. Effect of Electrolyte Composition | 61 |
| 5.2.2. Crystallography of Electrodeposited Metallic Powders | 64 |
| 6. CONCLUSION | 69 |
| REFERENCES | 71 |

LIST OF TABLES

TABLES

| | |
|---|----|
| Table 1.1. Global Diamond Supply by Application [8] | 3 |
| Table 3.1. The levels of copper sulfate bath composition and operating conditions | 24 |
| Table 3.2. Levels of cobalt sulfate bath composition and operating conditions | 27 |
| Table 4.1. Powder numbers according to electrodeposition parameters | 40 |
| Table 5.1. Compositions of electrodeposited metallic powders | 66 |

LIST OF FIGURES

FIGURES

| | |
|--|----|
| Figure 1.1. Schematic view of sawblade and cutting sockets..... | 1 |
| Figure 1.2. Diamond tool production processes [5] | 2 |
| Figure 1.3. Copper demand dynamics by source [9] | 4 |
| Figure 1.4. Distribution of cobalt demand worldwide as of 2016 [10] | 4 |
| Figure 1.5. Future availability and supply of raw materials [12] | 5 |
| Figure 1.6. Recycling rates of some metals [12] | 6 |
| Figure 2.1. Typical polarization curve for electrodeposition [19]..... | 10 |
| Figure 2.2. Schematical view of electrode surface area [22]..... | 13 |
| Figure 2.3. Schematic representation of recovery methods of valuable particle embedded waste cutting tools | 19 |
| Figure 3.1. Profile changes of electrodes after 1 hour of electrolysis, for assemblies employing anodes without the mask [35] | 22 |
| Figure 3.2. Profile changes of electrodes after 1 hour of electrolysis, for assemblies employing anodes with the mask[35] | 22 |
| Figure 3.3. Diamond cutting tool anode | 23 |
| Figure 3.4. Potential sweeps of cathode relative to Hg-Hg ₂ Cl ₂ electrode under; stirred and non-stirred conditions in copper sulfate bath..... | 24 |
| Figure 3.5. A picture of experimental set-up used in the recycling of diamond embedded copper-tin matrix cutting tools | 25 |
| Figure 3.6. Linear Sweep Voltammetry of Cobalt-Copper-Tin Matrix Cutting Tools | 27 |
| Figure 4.1. SEM images of collected diamond particles | 29 |
| Figure 4.2. SEM images of collected tin powders..... | 30 |
| Figure 4.3. Main effects plot for specific surface area of electrodeposited copper powder | 33 |

| | |
|---|----|
| Figure 4.4. Interaction plot for specific surface area of electrodeposited copper powders | 34 |
| Figure 4.5. Contour plots for specific surface area of electrodeposited copper powder | 36 |
| Figure 4.6. Effect of electrolysis parameters on particle size of deposited Cu powder | 37 |
| Figure 4.7. Specific surface area and particle size variance of collected metallic powders with respect to electrodeposition conditions | 40 |
| Figure 5.1. SEM pictures of copper deposits obtained at (a) 8.37 A/dm ² and (b) 10.46 A/dm ² current density, in 10g/L Cu ²⁺ and 0.25 M H ₂ SO ₄ electrolyte at 30°C | 44 |
| Figure 5.2. SEM picture of copper deposits obtained at 12.5 A/dm ² current density, in 10g/L Cu ²⁺ and 0.25 M H ₂ SO ₄ electrolyte at 30°C | 45 |
| Figure 5.3. SEM picture of copper deposits obtained at 8.37 A/dm ² current density, in 10g/L Cu ²⁺ and 0.25 M H ₂ SO ₄ electrolyte at 20°C | 46 |
| Figure 5.4. SEM picture of copper deposits obtained at 8.37 A/dm ² current density, in 10g/L Cu ²⁺ and 0.25 M H ₂ SO ₄ electrolyte at 30°C | 47 |
| Figure 5.5. SEM picture of copper deposits obtained at 8.37 A/dm ² current density, in 10g/L Cu ²⁺ and 0.25 M H ₂ SO ₄ electrolyte at 40°C | 47 |
| Figure 5.6. SEM pictures of copper deposits obtained in (a) 10g/L Cu ²⁺ and (b) 15g/L Cu ²⁺ , at 10.46 A/dm ² current density, in 0.5 M H ₂ SO ₄ electrolyte, at 30°C | 49 |
| Figure 5.7. Relative concentration of hydrogen ions as a function of sulfuric acid and total copper concentrations, at 25°C [54]..... | 50 |
| Figure 5.8. SEM pictures of copper deposits obtained in (a) 0.25 M and (b) 1 M H ₂ SO ₄ at 10.46 A/dm ² current density, in 15g/L Cu ²⁺ electrolyte at 30°C..... | 51 |
| Figure 5.9. Rietveld analysis of electrodeposited copper powders by using Maud software | 53 |
| Figure 5.10. XRD patterns of electrodeposited copper powders produced at constant 12.5 A/dm ² current density and 10 g/L constant copper ion concentration of electrolyte with two temperature and acid concentration of electrolyte | 54 |

Figure 5.11. XRD patterns of electrodeposited copper powders produced at constant 15 g/L copper ion concentration at 40°C constant temperature with two different current density and acid concentration of electrolyte 55

Figure 5.12. XRD patterns of electrodeposited copper powders produced at constant 1M acid concentration of electrolyte and 40°C constant temperature with two different current density and copper ion concentration of electrolyte..... 56

Figure 5.13. SEM pictures of (a) cobalt-copper-tin, (b) and (c) cobalt deposits obtained at 50 A/dm² current density, in 10 g/L Co²⁺ and 0.5 M H₂SO₄ electrolyte at 30°C .. 58

Figure 5.14. SEM pictures of (a)cobalt-copper-tin and (b) cobalt deposits obtained at 70 A/dm² current density, in 10 g/L Co²⁺ and 0.5 M H₂SO₄ electrolyte at 30°C 58

Figure 5.15. SEM pictures of (a) cobalt-copper-tin and (b) cobalt deposits obtained at 70 A/dm² current density, in 10 g/L Co²⁺ and 0.5 M H₂SO₄ electrolyte at 40°C 60

Figure 5.16. SEM pictures of (a) cobalt-copper-tin, (b) and (c) cobalt deposits obtained at 70 A/dm² current density, in 20 g/L Co²⁺ and 0.5 M H₂SO₄ electrolyte at 30°C .. 62

Figure 5.17. SEM pictures of (a) cobalt-copper-tin and (b) cobalt deposits obtained at 70 A/dm² current density, in 10 g/L Co²⁺ and 0.25 M H₂SO₄ electrolyte at 30°C 64

Figure 5.18. Rietveld analysis of electrodeposited cobalt-copper-tin powders at 70 A/dm² current density, in 10 g/L Co²⁺ and 0.5 M H₂SO₄ electrolyte at 30°C by Maud program..... 65

Figure 5.19. Rietveld analysis of electrodeposited cobalt-copper-tin powders at 70 A/dm² current density, in 20 g/L Co²⁺ and 0.5 M H₂SO₄ electrolyte at 30°C by Maud program..... 65

Figure 5.20. X-Ray diffraction patterns of electrodeposited metallic powders in (a) 20 g/L Co²⁺ and (b) 10 g/L Co²⁺, 0.5 M H₂SO₄ electrolyte at 70 A/dm² current density, at 30°C 67

CHAPTER 1

INTRODUCTION

Diamond and other valuable abrasive particle embedded composite cutting tools are preferred tools in industry because of their superior properties like high hardness, wear resistance, low friction coefficient, small affinity to nonferrous metals and low coefficient of thermal expansion. Not only hard metal cutting, drilling, polishing and grinding operations but also nonmetallic materials like marble, stone etc. could be done with diamond cutting tools [1]. They also provide high work piece quality, high productivity and reduced cost for machining of materials. Diamond and hard particle embedded cutting tools can be produced by various methods like cold pressing + sintering, hot pressing, brazing, infiltration and electrodeposition. When comparing sintering as powder metallurgy technique with electrodeposition, while sintering provides uniform impregnation of hard particles in the whole bulk with easier and cheaper process; only a monolayer of the particles to the surface of cutting tool can be manufactured by electrodeposition [2].

These harsh particles embedded abrasive parts are placed to the circumference of the metal disc to form a saw blade as it can be seen in Figure 1.1. In general, various metals and alloys like cobalt, copper, tin and up to 20% diamond particles and/or tungsten carbide are the main constituents of cutting tools [3].

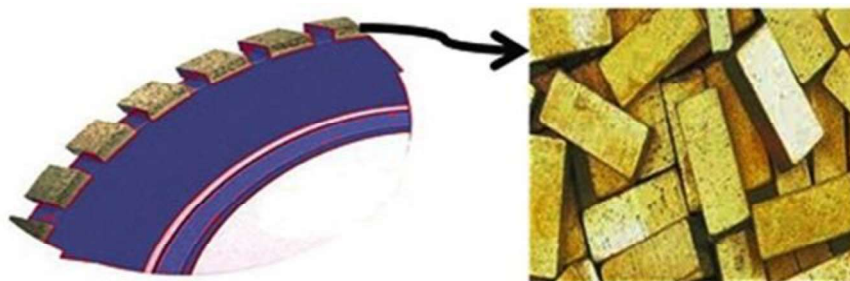


Figure 1.1. Schematic view of sawblade and cutting sockets

The mission of diamond and other valuable hard particles mission is grinding. Therefore, bonding of these particles to the metal matrix is crucial, because developing forces are bear up especially at the interfacial region. Chemical bonding provides higher durability, better grinding performance and longer lifetimes. In addition to that powder metallurgy (PM) avoids excessive chemical interaction between metal phase and diamond accordingly graphitization, so PM technology (see Figure 1.2) is the essential process for the production of diamond cutting tools [4].

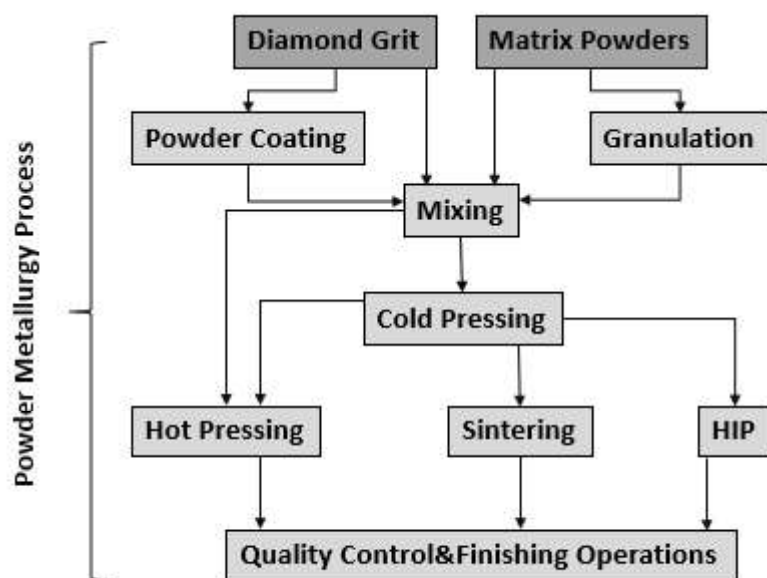


Figure 1.2. Diamond tool production processes [5]

Selection of metal matrix for the cutting tools should be appropriate for the material to be cut, polished or ground. For example, tungsten bond is chosen for highly abrasive materials like concrete, SiC, Si₃N₄, Al₂O₃; cobalt bond is used for granites; bronze, cobalt bond is employed for marbles etc. There are various matrix types as described previously; however, cobalt is primarily used constituent because of its ductility, compatibility, abrasion resistance and hardness in addition to providing stable bonding of diamonds. On the other hand, new researches have primarily focused on finding an alternative metal despite cobalt or at least decreasing its composition, because it is an expensive, hazardous and strategic metal. Other metals in the matrix like Cu, Sn, brass

and bronze are used to fill the pores coming from sintering however, they do not provide bonding to the diamond due to lower chemical affinity to carbon [6].

Increased mining restriction in various countries is the major driving force for the promotion of synthetic diamonds in the global market. In addition, rising demand for end use applications such as in electronics and super abrasives industry are some of the key factors for propelling the growth of synthetic diamond further in the global market [7]. According to global diamond supply by application (see Table 1.1), in 2013; almost all the produced diamonds were used for abrasive applications. The same table also shows that diamond recycling in abrasive applications is almost none [8].

Table 1.1. *Global Diamond Supply by Application [8]*

| Global Diamond Supply by Application (2013 Estimates in million carats) | | |
|--|---------------------|-----|
| <i>Gem Quality (Jewelry Application)</i> | | |
| <i>Mine Production</i> | 30 ct. | 92% |
| <i>Synthetic Production</i> | <1 | 2% |
| <i>Recycled/Buy-backs(polished)</i> | 2 | 6% |
| <i>Gem Quality (High-Tech Industry Application)</i> | | |
| <i>Mine Production</i> | 0 ct. | 0% |
| <i>Synthetic Production</i> | dependent on demand | N/A |
| <i>Industrial/Bort Quality (Abrasive Application)</i> | | |
| <i>Mine Production</i> | 100 ct. | 2% |
| <i>Synthetic Production</i> | 4,500 | 98% |
| <i>Recycled/Buy-backs(polished)</i> | N/A | 0% |

One of the materials used in the majority of cutting tools' metal matrix is copper. Metallic copper is produced in many countries like Chile, China, Peru etc. Copper is extensively used in many applications as shown in Figure 1.3 and copper demand for industrial machinery and equipment is growing day by day [9].

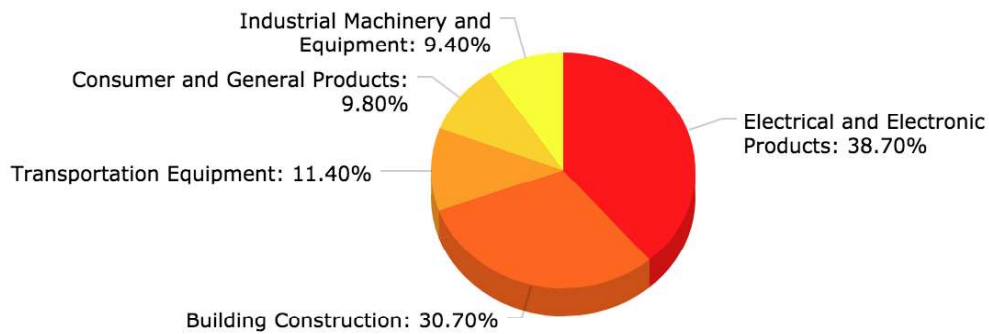


Figure 1.3. Copper demand dynamics by source [9]

The distribution of cobalt demand worldwide as of 2016 is represented in Figure 1.4. It is clearly shown that 10% of the cobalt is used in diamond drills [10].

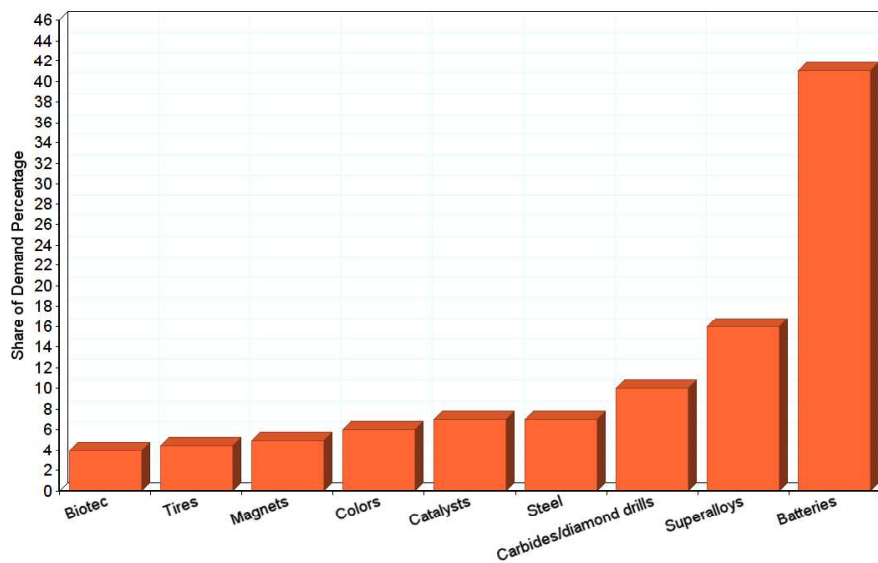


Figure 1.4. Distribution of cobalt demand worldwide as of 2016 [10]

About 80 % of copper production comes from the processing of the minerals of this metal. The remaining of 20 % is provided by recycling of copper from wastes as it can be seen Figure 1.5 and Figure 1.6 [11]. According to CUTEC Study (2016) reports copper reserves will supply copper demand by 2054 and future availability fall critical

material category [12]. As one of the other main metal matrix constituents of cutting tools, cobalt is also suffered from depletion. Cobalt reserves will supply demands until 2072 and it is classified as critical material category from CUTEC Study in Figure 1.5 [12]. Also, recycling rates of these metals are shown in Figure 1.6. As it can be deduced, the recycling rate is insufficient to meet the order when considering the supply demand ratio.

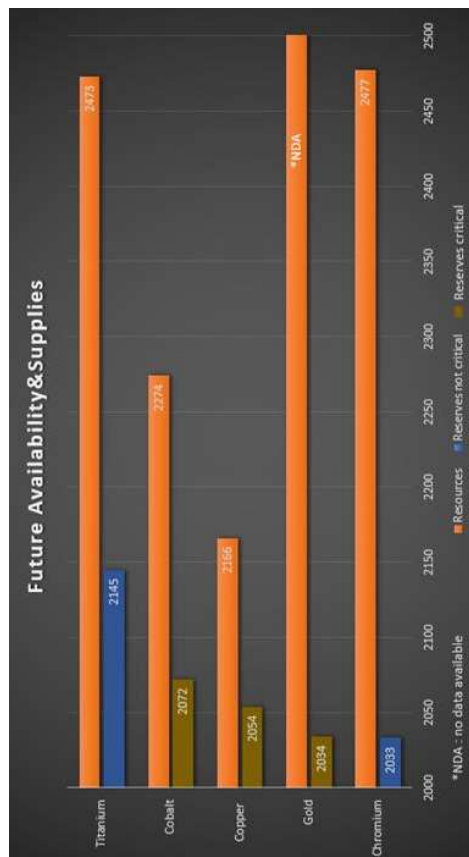


Figure 1.5. Future availability and supply of raw materials [12]

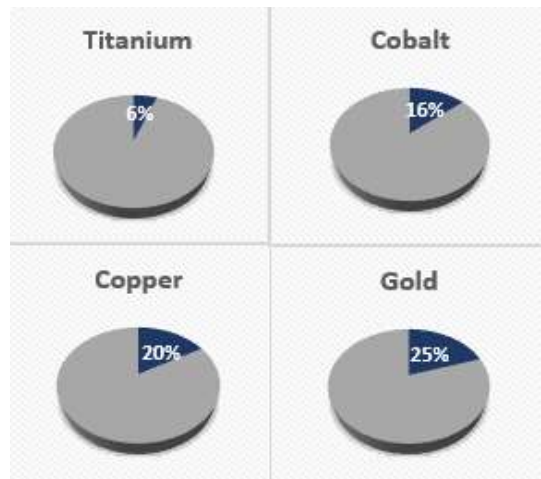


Figure 1.6. Recycling rates of some metals [12]

1.1. The Purpose of the Thesis

Normally a sawblade can be used for processing around 400 m² of stones. According to some researches 10% of the existing diamonds and metal residue could still remain in the teeth of discarded sawblades [6, 7]. Therefore, in waste diamond tools residual diamond particles and combined metallic agents are not consumed. For now, recycling diamond tools includes acid dissolution methods. The methods mainly involve; decomposition of metallic parts in potassium chlorate, hydrochloric acid and nitric acid. Filtration of valuable particles is done after dissolution of cutting tools and the solution that carries dissolved metal ions are discarded. Also, another disadvantage of this method is that the processes are relatively long and recycling efficiency is low [13].

This study offers recovery of the discarded diamond cutting tools. Not only diamond and other valuable particles were recovered, but also metals were recycled by co-deposition of metal powders in the study. The waste diamond tools used as anode were dissolved by applying power in relatively weak acidic electrolyte. While valuable particles that sink to the bottom of the electrolyte were collected after filtration so that they could be used again. Metal ions go into solution and collected as a powder at the cathode. Electrolysis provides collection of metal powders of various surface

morphology, shapes and sizes. This variation in morphology and size of powder strongly depend on the conditions such as the type of the electrolyte, metal being deposited, temperature, pH, current density etc.

The purpose of this study was to gain valuable particles and metals form cutting tools as a powder and optimize parameters that affect the morphology, density and specific surface area of electrochemically collected metallic powder. Furthermore, it is aimed that laboratory scale results of this study may give directions to industrial applications. Thus, the knowledge and practice principles of integrated recycling for depleted sources such as for metals and diamonds in scrap sockets, instead of being thrown away may be applied.

CHAPTER 2

LITERATURE REVIEW

2.1. Electrodeposition of Metallic Powders

Mechanical comminution, chemical reaction, electrolysis and liquid metal atomization are the different methods used in industry for production of metallic powders [14]. With easy operation route and low capital investment electrochemical production of metallic powder is an economical way. When comparing with other production methods, electrolysis provides production of high purity metal powder with low oxygen content which can be easily pressed and sintered [8, 9]. Also, production in a closed circuit and more environmental friendly approach with respect to others makes electrolysis a sensible and usable method [16]. Metal powders can be produced galvanostatically and potentiostatically by means of electrolysis. However, formation of compact, low surface area and relatively passive surface morphology powders require close control of electrolysis conditions that vary with available parameters.

2.1.1. Potentiostatic and Galvanostatic Powder Electrodeposition

According to studies in the literature, powdered deposits can be attained at all potentials that correspond to limiting current density plateau if sufficiently high deposition time is given [17]. The current density values which are equal to and greater than limiting current density in galvanostatic deposition and current density values corresponding to the critical current density namely j_{cr} in potentiostatic deposition can be used to form electrolytic metallic powder. Since the effect of small change of current densities cause a large change in the overpotential, limiting diffusion current plateau covers a wide range of overpotentials, therefore the electrolytic metal powder cannot be confined to a specific current density value [18]. There are three regions of overpotential to get compact, rough and powdered deposits as shown in Figure 2.1.

According to the literature, there are two critical overpotential values, these are the critical overpotential for dendrite growth initiation, η_i and the critical overpotential for powder formation, η_c . Dendritic deposits can be obtained at all overpotentials between η_i and η_c if sufficiently long deposition time is given as stated previously [19].

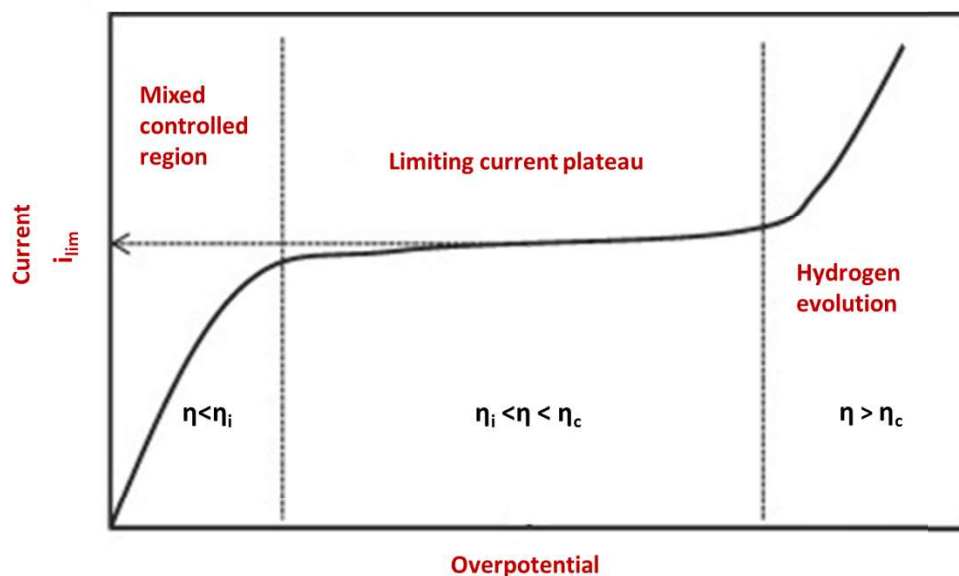


Figure 2.1. Typical polarization curve for electrodeposition [19]

According to Popov et al. [19], the minimum overpotential at which dendritic growth initiation η_i , is possible at macroelectrode is expressed by;

$$\eta_i = \frac{b_c}{2.3} \ln \frac{4j_L}{j_0} + \Delta\eta \quad (1)$$

And minimum overpotential at which instantaneous powder formation η_c , is expressed by;

$$\eta_c = \frac{b_c}{2.3} \ln \frac{j_L \delta}{j_0 h_0} + \Delta\eta \quad (2)$$

where b_c is the cathodic Tafel slope, j_L is the limiting diffusion current density, j_0 is the exchange current density, δ is the diffusion layer thickness, and h_0 is the initial protrusion height.

$\Delta\eta$ in Eqs. 1 and 2 represents the difference between reversible potential of the tip of the dendrite and planar surface and is given by;

$$\Delta\eta = \frac{2\sigma V}{nFR} \quad (3)$$

where nF is the number of Faradays per mole of consumed ions, R is the tip radius, V is the molar volume of deposited metal, and σ is the interfacial energy between metal and solution. $\Delta\eta$ is in the order of a few millivolts therefore it can be neglected in the consideration of both η_i and η_c overpotentials expressions as follows;

$$\eta_i = \frac{b_c}{2.3} \ln \frac{j_L}{j_0} \quad (4)$$

$$\eta_c = \frac{b_c}{2.3} \ln \frac{j_L \delta}{j_0 h_0} \quad (5)$$

The relationship between overpotential and current density in mixed controlled metal electrodeposition is stated by;

$$\eta = \frac{b_c}{2.3} \ln \frac{j}{j_0 (1-j/j_L)} \quad (6)$$

where j is the current density of the electrodeposition.

Current densities j_{cr} and j_i , corresponding to overpotentials η_c and η_i can be obtained by eliminating η from equation 1,2 and 6 as follows;

$$j_i = 0.8j_L \quad j_{cr} = \frac{j_L(\delta/h_0)}{1 + (\delta/h_0)} \quad (7)$$

for $\delta/h_0 \gg 1$. As a result, dendritic growth is not possible at [20];

$$j < j_i \quad (8)$$

But growth is possible after an induction time at

$$j_i \leq j < j_L \quad (9)$$

And instantaneous growth is possible at

$$j \geq j_L \quad (10)$$

in potentiostatic electrodeposition.

In galvanostatic electrodeposition, these conditions will be in opposite direction. In galvanostatic deposition, surface roughness amplification of a protrusion with an initial height h_0 obeys the same relation with potentiostatic electrodeposition [21,22];

$$h = h_0 \exp(t/\tau) \quad (11)$$

where $\tau = (\delta^2 / V_m D C_0)$ if the condition $\delta \gg h$ is satisfied, D is diffusion coefficient, C_0 is the bulk concentration and t is time.

Figure 2.2 represents electrode surface and the real surface area of electrode will increase with time according to;

$$S = S_0 \exp(t/\tau) \quad (12)$$

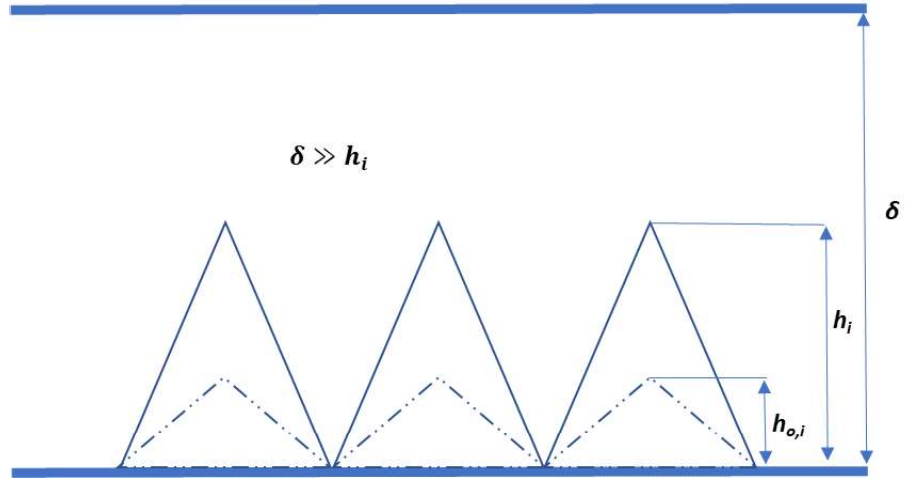


Figure 2.2. Schematical view of electrode surface area [22]

Since,

$$S = k \sum_{i=1}^N h_i \quad (13)$$

$$S_0 = k \sum_{i=1}^N h_{o,i} \quad (14)$$

Therefore, overpotential can be obtained by substitution of j , where;

$$j = j^0 \exp(-t/\tau) \quad (15)$$

into equation 6, and j^0 is the initial current density,

$$\eta = \frac{b_c}{2.3} \ln \frac{j^0 \exp(-t/\tau) j_L}{j_0 [j_L - j^0 \exp(-t/\tau)]} \quad (16)$$

Substitution of h from equation 11 in equation 5 shows the change of critical overpotential of instantaneous dendritic growth with time caused by nondendritic surface roughness amplification as;

$$\eta_{c,t} = \frac{b_c}{2.3} \ln \frac{j_L \delta}{j_0 h} = \eta_c - \frac{b_c}{2.3} \frac{t}{\tau} \quad (17)$$

In galvanostatic electrodeposition conditions, nondendritic elaboration causes a decrease in the critical overpotential for dendritic growth according to equation 16, but at the same time the overpotential of deposition decreases according to equation 15. The time t_i in which these two overpotentials become equal can be gained by the elimination of η from equation 15 and 16 as;

$$t_i = -2.3\tau \log \frac{j_L}{j^0} \quad (18)$$

if $\delta \gg h_0$. Hence, $t_i = 0$ for $j_0 = j_L$ and instantaneous dendritic growth is possible; at $j^0 < j_L$ for $t_i < 0$ dendritic growth is not possible. In this way, the induction period for the dendritic growth becomes equal to transition time and this discussion is valid for galvanostatic powder electrodeposition.

2.1.2. Surface Area of Electrodeposited Metal Powders

Specific surface, apparent density, flowability, particle grain size and particle size distribution are key properties that determine qualification of metal powder. All these properties can be related to the electrodeposition conditions.

The specific surface of a powder and a powdered deposit is expressed as the surface area per unit of the mass of powder.

The overpotential in the activation-diffusion control region, η is defined as follows;

$$\eta = \frac{b_c}{2.3} \ln \frac{j}{j_0} + \frac{b_c}{2.3} \ln \frac{1}{1 - \frac{j}{j_L}} \quad (19)$$

This formula is the summation of the activation overpotential, η_{act} , (part of the given expression before the summation sign) and diffusion overpotential, η_{diff} , (part of the given expression after the summation sign). And if $j \rightarrow j_L$, η_{act} becomes;

$$\eta_{act} = \frac{b_c}{2.3} \ln \frac{j_L}{j_0} \quad (20)$$

Therefore, this term is equal to critical overpotential for the initiation of dendritic growth [23]. Simultaneously as $j \rightarrow j_L$, $\eta_{diff} \rightarrow \infty$.

Very small increase of current density in the limiting current density range causes a dramatic increase in deposition overpotential. Regardless of electrodeposition overpotential, the charge transfer overpotential and the ohmic drop in the solution remain the same for all overpotentials corresponding to limiting diffusion current density plateau. Because charge transfer overpotential and ohmic drop are only dependent on the current density. While, in the limiting diffusion current density range, increasing deposition overpotential brings about strong increasing of dispersity and accordingly increasing surface area of metal deposits. Therefore difference in overpotentials of deposition is correlated to increasing surface area of deposited metals by formulation [24]. Therefore, the following equation can be driven for the direct determination of the energy of dispersed solid metal surface formation in solutions.

$$\gamma = \frac{(\eta_2 - \eta_1) \int_0^t I dt}{(S_2 - S_1)} \quad (21)$$

where I is applied current of electrodeposition, t is the time of electrodeposition, $\int_0^t I dt$ is the quantity of charge passed, η_2 and η_1 are overpotentials of electrodeposition belonging to the limiting diffusion current density range, S_2 and S_1 are the surface area of dispersed deposits at the overpotentials η_2 and η_1 , respectively, and γ is the surface energy of dispersed deposit formation.

For $\eta_2 > \eta_c$, $\eta_1 > \eta_i$ and $S_2 \gg S_1$, equation 20 can be rewritten in the form;

$$S_2 = \frac{(\eta_2 - \eta_1) \int_0^t I dt}{\gamma} \quad (22)$$

The quantity of electrodeposited metal, m , is expressed by;

$$m = \frac{M}{nF} \int_0^t I dt \quad (23)$$

assuming the current efficiency for metal electrodeposition $\eta_1(M)$ to be 100%, where M is the atomic mass of deposited metal. Therefore, specific powder surface S_{sp} can be calculated from the following equation.

$$S_{sp} = \frac{(\eta_2 - \eta_1)nF}{\eta_1(M)\gamma M} \quad (24)$$

2.1.3. Particle Size and Apparent Density of Electrodeposited Metal Powders

Electrodeposited metal powders can not be formed to have identical geometry. Individual particles have various forms and very different surface areas for the same average size of granule [25]. The regime of electrolysis, composition of solution, deposition time, cathodic material, temperature and hydrodynamic regime are quite influential for size and shape of powder particles. The characteristics of electrodeposition processes strongly depend on hydrogen evolution. Also, the type of cathodic materials used had strong effect on the shape, particle size and particle size distribution [26].

Mass per unit volume of powder is the definition of the apparent density. Electrolyte composition, electrolyte temperature, electrolyte circulation rate, current density etc. affect the apparent density of electrodeposited powders. The dependence of the apparent density on the specific surface of a copper powder can be calculated using the data of Calusaru [27]. The relationship between apparent density, ρ' and the specific surface of a powder can be expressed by;

$$\rho' = \frac{K}{S_{sp}} \quad (25)$$

Where K is a constant and $K \approx 1,000 \text{ cm}^{-1}$ [28].

2.1.4. Hydrogen Co-Deposition

Morphological forms of deposited metal powders such as dendrite, needle, spongy, fibrous, honeycomb-like structure etc. also strongly depend on hydrogen codeposition during electrodeposition processes [29, 30]. According to its application area, these forms may be useful or undesirable. For example, while the creation of open and porous structures suitable for electrodes in electrochemical devices but it is not applicable for batteries. In case of metal deposition, irregular or disperse deposits are formed at current densities and overpotentials which corresponds to the plateau of the limiting diffusion current density and at higher values, where hydrogen evolution reaction occurs together with metal electrodeposition. According to all studies about morphology of metal electrodeposition, the shape of the metal powder strongly depends on the quantity of evolved hydrogen. For example, honeycomblike structure was obtained only under a quantity of evolved hydrogen which was high enough to change hydrodynamic conditions near the electrode layer. However, if the quantity of evolved hydrogen was below the critical value to change hydrodynamic conditions near the electrode powder particles deposited were dendritic in shape, and if the quantity of evolved hydrogen was above the critical value metal powders could be formed as cauliflower-like [31].

2.2. Cutting Tools and Importance of Cutting Tools Materials Recycling

In 1883, Gay developed the idea of producing abrasives by adding quartz into the metal matrix. In the same way, using the iron, brass and steel powders, the matrix could be made by powder metallurgy techniques such as hot pressing and infiltration. These ideas of Gay found the industrial application area in 1940 by increasing the development of diamond cutting tools. Instead of using rare diamonds, synthetic diamond production started in 1955 with the increase of demand for usage of diamond

in the industry due to its superior properties over other cutting tools. After General Electric announced that synthetic diamonds could be produced in industrial scale, the developments accelerated. Initially, synthetic diamonds could only be produced as small parts but nowadays even they can be produced to cover the surface of the material. The methods of making diamond tools have undergone a fantastic development since the invention of the synthetic diamond and in the last 50 years, after synthetic diamond commercialization, high-quality metal matrix cutter production has begun [32].

As it is known, depletion and rarity of natural sources lead scientists to recycling and recycling studies have gained importance. From the examination of the application areas and demand of these cutting tools in industry, it can be realized that; recovery of cutting tools can contribute to global economy, environment and manufacturers.

2.3. Current Methods of Recovering Valuable Particle Embedded Cutting Tools

Currently, the general processes of recycling diamond tools used in industry involve acid dissolution and these processes adopt the same separation principle by utilizing the characteristics of diamond and tungsten carbide, which are insoluble in acid, while other metals are soluble. After the filtration of valuable particles, the solution that carries dissolved metal ions are discarded [33]. These methods are hazardous to the environment and human health, because solutions contain high concentrations of metal ions and acids. Also, acid decomposition methods take more time and recycling efficiency is low. To make comparison, current recovery methods and electrolytic recovery method used in this study are summarized and shown in the following Figure 2.3.

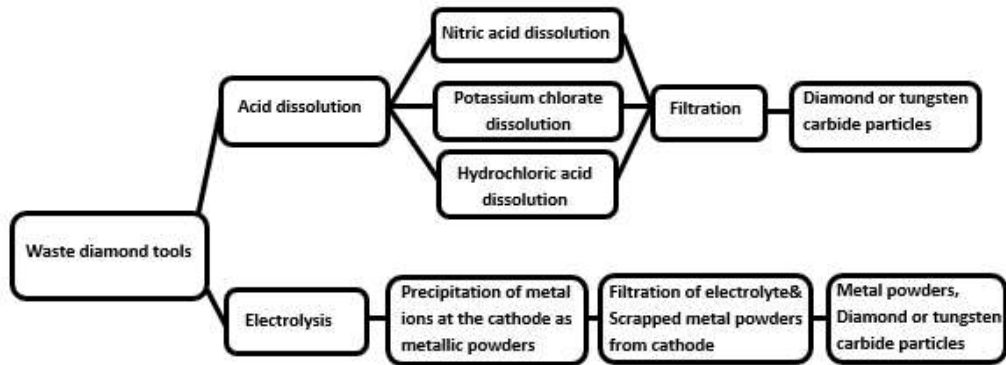


Figure 2.3. Schematic representation of recovery methods of valuable particle embedded waste cutting tools

Also, there is some academic studies about recycling of the diamond embedded cutting tools with different matrix compositions by electrolysis. These studies involve acid leaching of discarded cutting tools and after recovering diamond, acid leaching solution used as electrolyte. Metal powders can be gathered from the cathode by utilizing different parameters, however acid concentration of solutions used for leaching was high [1,34].

CHAPTER 3

EXPERIMENTAL

3.1. Electrolytic Cell

Freshly prepared 100 ml of electrolyte which contained $\text{CuSO}_4 \cdot 5\text{H}_2\text{O}$ and H_2SO_4 was used for recovery of diamond embedded copper-tin matrix cutting tools in each experiment. The 100 ml of electrolyte which contained $\text{CoSO}_4 \cdot 7\text{H}_2\text{O}$ and H_2SO_4 was used for recovery of diamond embedded cobalt-copper-tin matrix cutting tools. The construction of the cell was based on the simulation of the electrodeposition process by using COMSOL Multiphysics software program. According to the results of the program shown in Figure 3.1 and Figure 3.2, some precautions were necessary to provide uniform decomposition of the anode, before starting the experiments. After 1 hour of electrodeposition process, anode thickness changes were shown from the right legend in Figure 3.1. Obviously, during 1 hour of electrolysis, 220 microns to 300 microns anode materials were dissolved. It means that nonhomogeneous dissolution occurred throughout the anode surface by oxidation of materials with the application of power. Especially, edges of the prismatic anodes, more dissolution occurred due to edge effect. At sharp edges, electric current tends to concentrate at the edge of the anode. With the same logic, the metal layer deposition of edges became thicker than the central area of the cathode according to left-hand side legend. Contrary to Figure 3.1, with the application of mask to anode material, uniform thickness changes was obtained in Figure 3.2. Therefore, to avoid excessive dissolution of the anode edges that of the prismatic in shape, anodes were masked with epoxy.

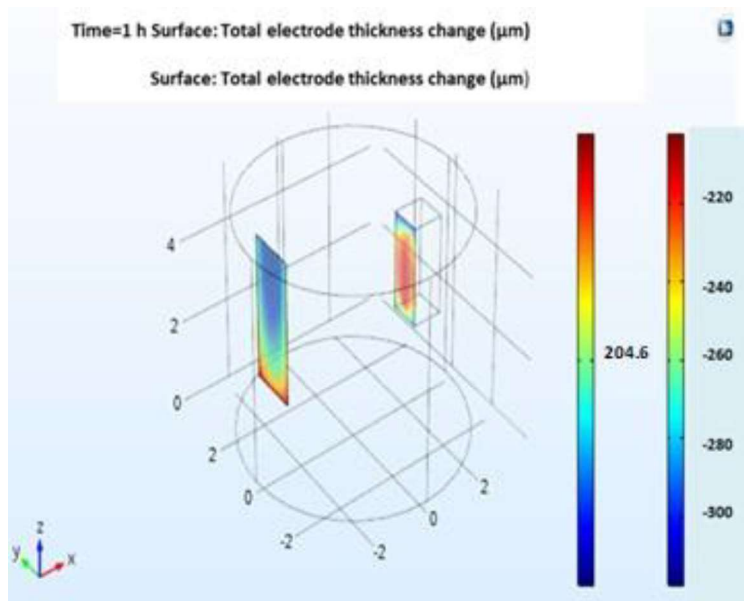


Figure 3.1. Profile changes of electrodes after 1 hour of electrolysis, for assemblies employing anodes without the mask [35]

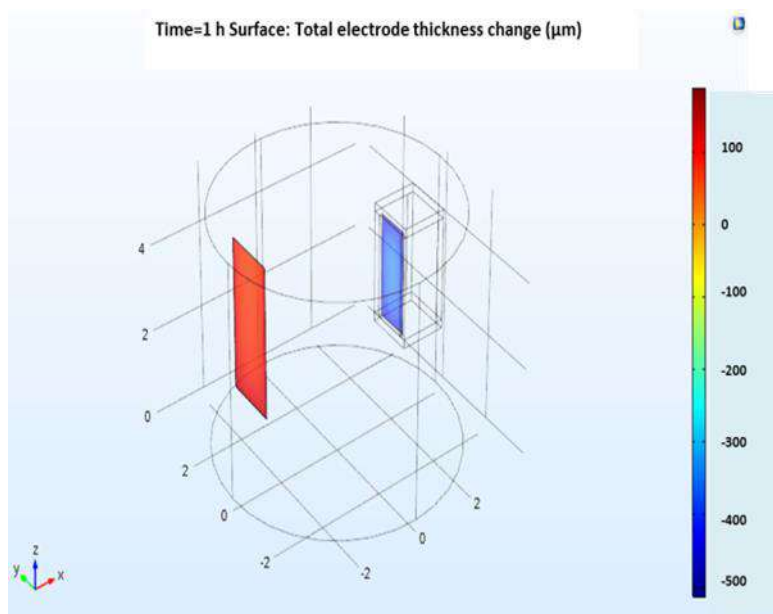


Figure 3.2. Profile changes of electrodes after 1 hour of electrolysis, for assemblies employing anodes with the mask[35]

Process equipment used for recovery of diamond cutting tools were Agilent B2901A Precision Source DC power supply, MTOPS HD180 Hot plate& Magnetic stirrer.

3.2. Recycling of Diamond Embedded Copper-Tin Matrix Cutting Tools

An electrochemical cell employing a rectangular surface of a waste diamond tool as anode, shown in Figure 3.3, and an AISI304 stainless steel sheet cathode was used in this study. Electrodes were immersed into the electrolyte having 0.1 to 0.3 molar CuSO_4 and 0.25 to 1 molar H_2SO_4 at temperatures of 20 to 40°C.



Figure 3.3. Diamond cutting tool anode

To determine current density range to be operated, linear sweep voltammetry for copper deposition was done by using Gamry Instruments Reference 3000 potentiostat and curve is shown in Figure 3.4. Sweeps were done between 0-1.5 V and, scan rate was chosen 100 mV/s. Reference electrode was saturated calomel electrode for linear sweep voltammetry. Metal deposition process started at the cathode when the sharp fall of the current density occurred in the negative scan. The sweeps under stirred and non-stirred conditions are also compared in Figure 3.4. Stirring rate was 500 rpm in the stirred condition. Deposition process under stirred condition took place at more negative current densities than that of unstirred condition. In addition, the linear sweep curve under stirred conditions had steeper slope in the negative range. As it is known, these results showed that start of nucleation was more difficult and growth of electrodeposited nuclei was easier when solution was stirred [36]. As discussed before, in galvanostatic powder electrodeposition the initial deposition current density must be larger than the limiting diffusion current density, therefore in this study under

stirred condition 0.0837 A/cm², 0.1046 A/cm² and 0.125 A/cm² current density values were studied.

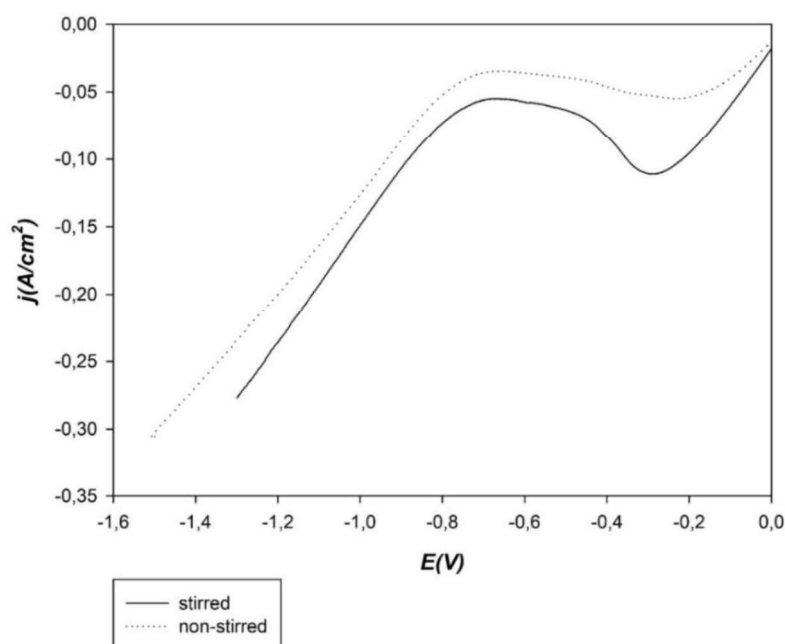


Figure 3.4. Potential sweeps of cathode relative to Hg-Hg₂Cl₂ electrode under; stirred and non-stirred conditions in copper sulfate bath

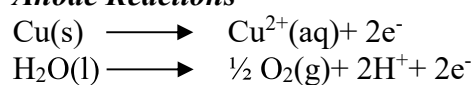
Process parameters are tabulated in Table 3.1. Full factorial design of experiments was used to evaluate the influence of process parameters on the electrodeposited metal powders characteristic with a feasible number of experiments. Full factorial design gave 3⁴ number of experiments with 3 different levels of 4 parameters.

Table 3.1. The levels of copper sulfate bath composition and operating conditions

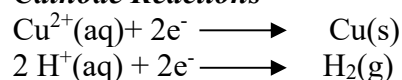
| | | | |
|---|------|-------|------|
| Temperature (°C) | 20 | 30 | 40 |
| Current Density (A/dm²) | 8.37 | 10.46 | 12.5 |
| Acid Concentration (M) | 0.25 | 0.5 | 1 |
| Cu Ion Concentration (g/L) | 10 | 15 | |

Electrodes were kept parallel to each other by using 3 cm inter electrode distance. Anode materials contained diamond particles embedded to an 85 % Cu and 15 % Sn containing prismatic shape. All experiments were performed for 3 hours, using 500 rpm stirring. After 3 hours of electrolysis, while galvanostatically deposited copper powders were scraped from the stainless-steel cathode easily, diamond and tin particles which sink to the bottom of the electrolyte were filtered from the electrolyte. Reactions that took place at anode and cathode are listed below.

Anode Reactions



Cathode Reactions



Collected copper powders were washed with ethanol for remaining sulfuric acid and then with 0.1 molar benzoic acid solution for remaining acid and preventing oxidation of copper powders. A picture of the experimental set-up is shown in Figure 3.5.



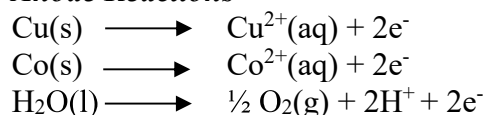
Figure 3.5. A picture of experimental set-up used in the recycling of diamond embedded copper-tin matrix cutting tools

3.3. Recycling of Diamond Embedded Cobalt-Copper-Tin Matrix Cutting Tools

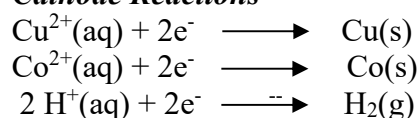
The same experimental set-up was used for experiments employing cobalt-copper-tin matrix cutting tool anodes. However, AISI 304 stainless steel cathodes were covered

by aluminum foil in these experiments, because cobalt is soluble in stainless steel as deduced from iron-cobalt phase diagram [37]. Anodic and cathodic reactions are given as follows:

Anode Reactions



Cathode Reactions



Linear sweep voltammetry was conducted by using Gamry Instruments Reference 3000 potentiostat as shown in Figure 3.6. For linear sweep voltammetry, sweep range was chosen as 0-8 V with 100 mV/s scan rate. Saturated calomel electrode was also reference electrode for this system. In the Figure 3.6, effect of electrolyte agitation on current density-potential scan is compared. Metal ion concentration was reduced with time when optimal hydrodynamic conditions dominated in the diffusion layer. Stirring provided transfer of metal ions to the cathode surface where reduction takes place, therefore, forced convection favored the metal reduction as time of electrodeposition progressed. The voltammogram of agitated condition showed that limiting diffusion current density increased when compared with voltammogram that was obtained under non-stirred condition, mainly due to easy ion transfer in the electrolyte caused descending of ion concentration near electrode layer. Consequently, at stationary condition limiting current density was easily reached. Therefore, according to linear sweep voltammetry results under stirred condition, 0.5 A/cm² and 0.7 A/cm² current density values were conducted for recycling of diamond embedded cobalt-copper-tin matrix cutting tools.

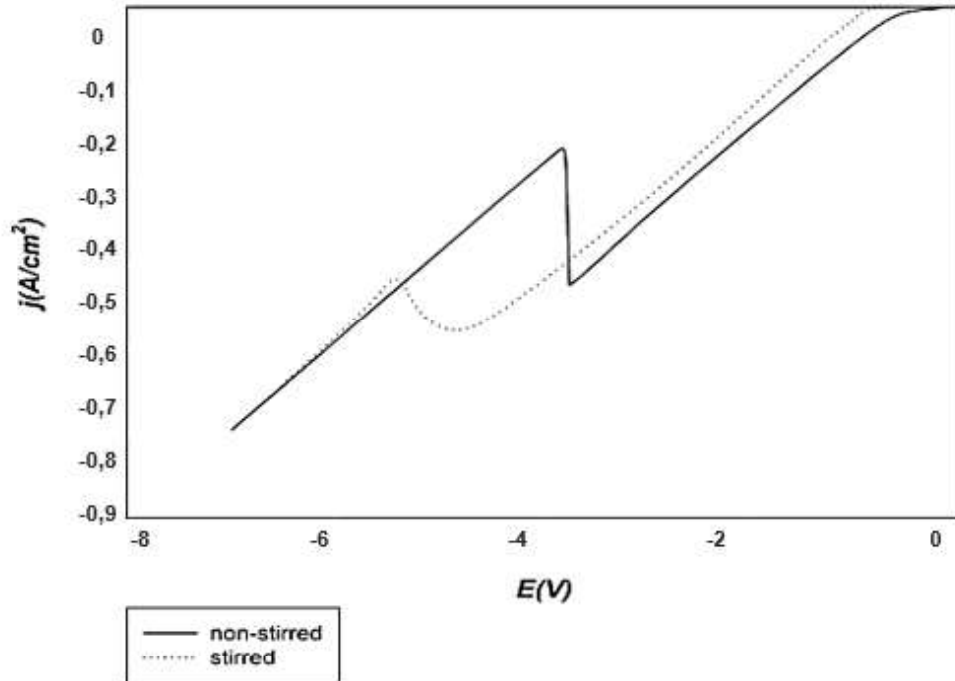


Figure 3.6. Linear Sweep Voltammetry of Cobalt-Copper-Tin Matrix Cutting Tools

For this set of experiments, electrodes were immersed into the electrolyte having 0.17 to 0.35 molar CoSO_4 , 0.25 to 0.5 molar H_2SO_4 at temperatures of 30 and 40°C. Levels of cobalt sulfate bath composition and operating conditions of electrodeposition are tabulated in Table 3.2. Full factorial design brought 2^4 number of experiments with 2 different variables of 4 parameters.

Table 3.2. Levels of cobalt sulfate bath composition and operating conditions

| | | |
|--|------|-----|
| Temperature(°C) | 30 | 40 |
| Current Density(A/dm²) | 50 | 70 |
| Acid Concentration(M) | 0.25 | 0.5 |
| Co Ion Concentration(g/L) | 10 | 20 |

Anode materials contained diamond particles embedded to an 80 % Co, 17% Cu and 3% Sn containing prismatic shape. Except electrolyte composition, anode and cathode materials, all other experimental design, electrodeposition time, mixing condition

were the same as the experiments performed for recycling of diamond embedded copper-tin matrix cutting tools.

3.4. Characterization of Collected Powders

All electrodeposited copper powders, collected tin powders and diamond were characterized by Nova NanoSEM 430 scanning electron microscopy (SEM) equipped with energy dispersive x-ray spectroscopy (EDX) unit. In addition, X-ray diffractions (XRD) of copper powders were taken to analyze the effects of electrolysis conditions on the crystallography of powders by Rigaku DMAX 2200 X-Ray Diffractometer, (equipped with a 3kW power generator and working at 40 mA and 40 kV, Cu K α radiation at a wavelength of 0.154183 nm was used as X-Ray sources, scan rate was selected 2°/min). Furthermore, specific surface area measurements of the collected copper powders were performed at room temperature using AUTOSORB_6B surface area and pore size analyzer. In addition, Mastersizer Hydro 2000S particle size analyzer was used to examine particle size distribution of electrodeposited metal powders.

CHAPTER 4

RESULTS

4.1. Recovery of Diamond Particles from Metal Matrix Composite Cutting Tools

Regardless of the anode, cathode, experimental set-up and experimental conditions, diamond particles were gathered from the bottom of the electrolyte after the experiments. During the electrolysis applied voltage caused the anodic components to dissolve as ions and these ions were reduced at the cathode. During oxidation (dissolution) of metals from anode, metal-diamond chemical or physical bonds were broken and due to the noble characteristics of diamond particles, they fell into the electrolyte. After the 3-hour experiments, free diamond particles were gathered by filtration of the electrolyte. SEM image of the collected diamond particles from a typical experiment is shown in Figure 4.1. The diamond particles were faceted with hexagonal or octahedral shapes and around 500 μm size.

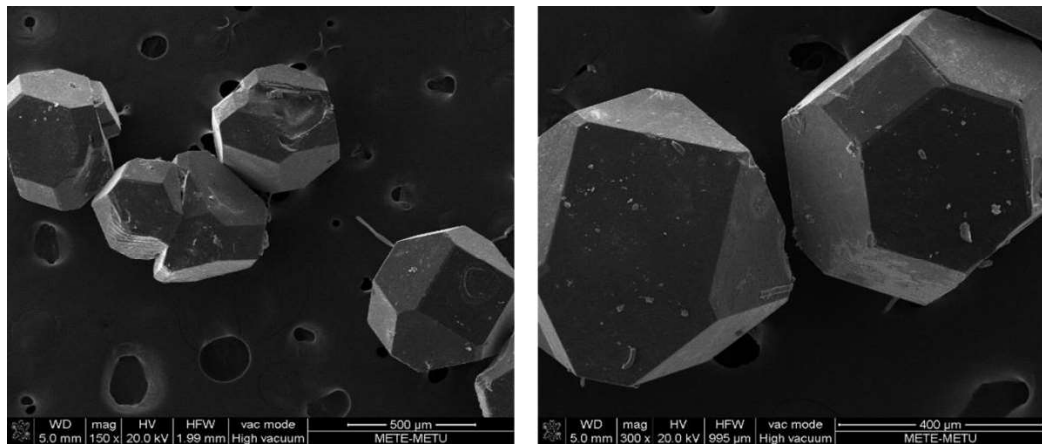


Figure 4.1. SEM images of collected diamond particles

4.2. Recovery of Metals from Cu-Sn Matrix Composite Cutting Tools

4.2.1. Tin Powders

In accord with the same logic as diamond particle collection, applied voltage was not enough to dissolve and deposit Sn powders. Therefore, tin powders sink to the bottom of electrolyte as anode materials were dissolved by electrolysis. While copper ions were forced to go into the electrolyte by the application of current, breaking of bonds between copper and other constituents like tin and diamond caused separation of tin powders from anode. Tin particles were dropped into solution mainly due to applying insufficient potential for oxidation/reduction of tin ions. SEM image of filtered Sn powders from the electrolyte is shown in Figure 4.2. As it can be seen from the general particle views, the edges and corners of the Sn powders could be clearly detected, and the average particle size was nearly 100-200 μm .

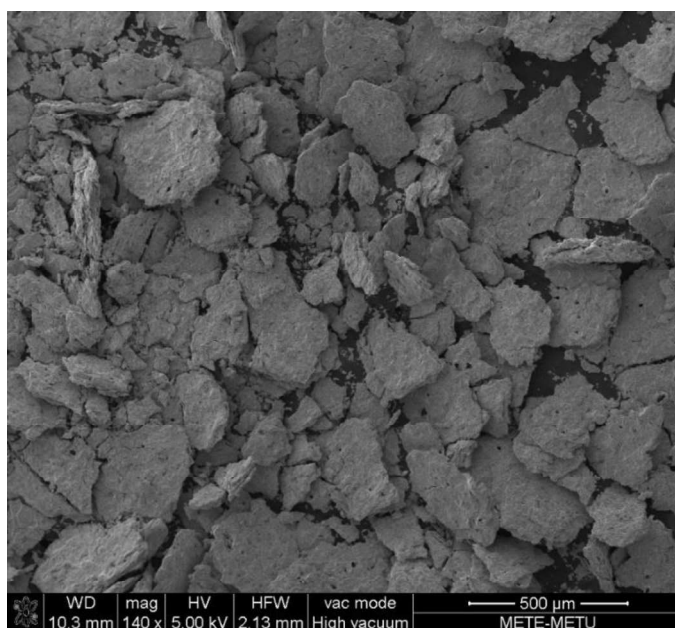


Figure 4.2. SEM images of collected tin powders

4.3. Specific Surface Area of Electrodeposited Copper Powder

Specific surface area is an important powder property defined as the total surface area of a powder per unit of mass with units of m^2/g [38]. In this thesis, every different parameter had great effect on the powder properties. Specific surface area was the

one of those properties; in addition to that smaller surface area to mass ratio was preferred for handling and sintering processes of metallic powders. The specific surface areas of powders were measured by the Brunauer, Emmett and Teller (BET) technique after collection of copper powders from stainless steel cathode.

A statistical experimental design was used to determine the effects of copper ion concentration of electrolyte, current density, temperature and sulfuric acid concentration to the specific surface. According to regression analysis, regression formula of specific surface area with respect to above mentioned parameters was derived and given in Equation 25.

Regression equation was used to describe the relationship between the response and the parameters in the model. The regression equation is an algebraic representation of the linear effects of parameters. In the regression equation, surface area values were the response variable, 0.336 was the constant or intercept, 0.0297 was the estimated coefficient for the current density parameter, and 0.02031, 0.0162 and the 0.002 were the coefficients for the temperature, copper ion concentration and the acid concentration of electrolyte respectively. The parameters that had decreasing effect on the surface area of electrodeposited copper powders yielded negative coefficients in the regression analysis given in Equation 25.

$$S. A. (m^2/g) = 0.336 + 0.0297 A - 0.02031 B - 0.0162 C + 0.002 D \quad (25)$$

where A: Current Density (A/dm^2), B: Temperature ($^{\circ}C$), C: Cu Ion Concentration (g/L) and D: Acid Concentration (M) of electrolyte.

The magnitudes of the coefficients indicated the weights of their effects. According to Equation 25, decreasing current density decreased surface area of electrodeposited copper powders by a factor of 0.0297. Another output of the regression formula is; increasing temperature had widening effect on the surface area of electrodeposited copper powders with a factor of 0.02031. The third outcome of the analysis is; addition of $CuSO_4 \cdot 5H_2O$ to the electrolyte which was one of the sources of copper ion, caused

decrease in surface area by a factor of 0.0162. It was also deduced from the analysis of the results that surface area of the copper powders remained almost constant with the addition of sulfuric acid to the electrolyte. On the other hand, slight increase was seen in the surface area values upon increasing acid concentration of electrolyte. It should be noted that, above equation was obtained for parameters within the limits covered in this study. All in all, the most effective parameters on the surface area of electrodeposited copper powders were current density, temperature and the copper ion concentration of the electrolyte with factors; +0.0297, -0.02031 and -0.0162 respectively.

Furthermore, the parameters that played important role or that were dominant on the surface area of the electrodeposited copper powders could be seen in Figure 4.3. In parallel to regression analysis, while the most powerful parameters were current density and the temperature, copper ion concentration of electrolyte followed them. Main effect plots supported regression analysis and interaction plot results that acid concentration of the electrolyte was not much effective in the surface area at 0.25 to 1 M range. But a slight increase observed in general with increasing acid concentration from 0.25 M to 1 M.

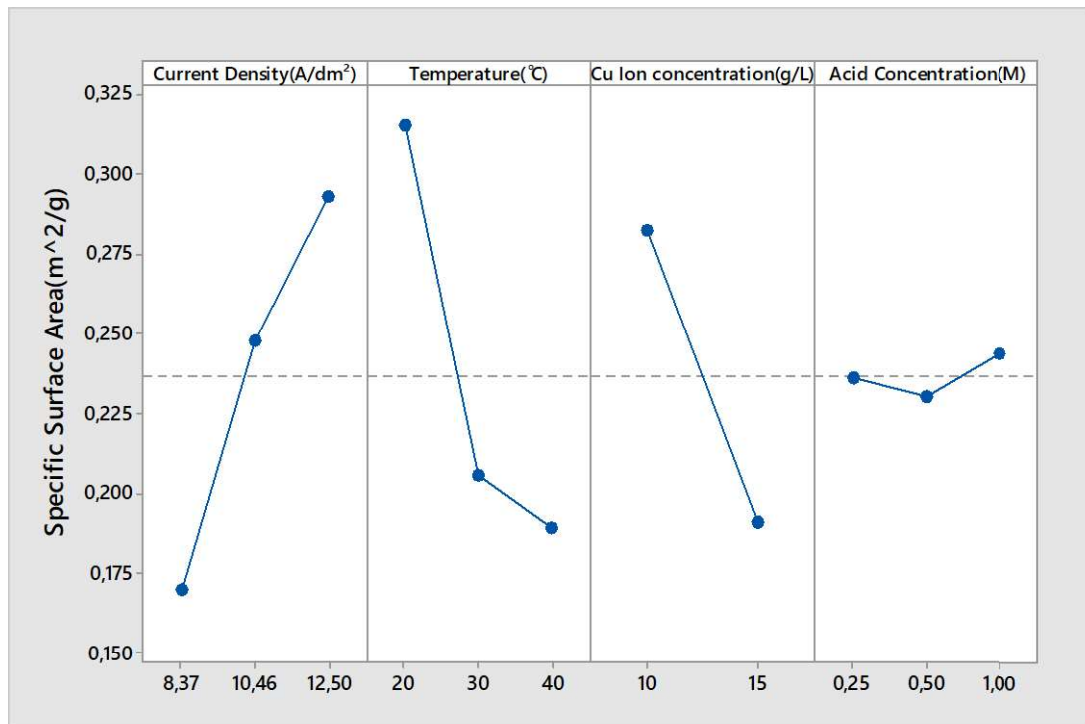


Figure 4.3. Main effects plot for specific surface area of electrodeposited copper powder

In addition, the results were subjected to factorial design analysis to obtain the interaction effects of the parameters on the specific surface area of powder, illustrated in Figure 4.4. As it can be seen from the interaction plot for specific surface area of electrodeposited copper powders, where vertical axes of all plots represent specific surface area values, parameters which were current density, temperature, Cu ion concentration and acid concentration of electrolyte represent the horizontal axes columns respectively. Interaction plot described not only the effect of a single parameter on the surface area but also how multiple parameters influenced the surface area at the same time. It could be deduced that while temperature and copper ion concentration of electrolyte had descending effect, current density and acid concentration of electrolyte had ascending effect on the specific surface area of the powders. At the first row; whatever the other parameters were (temperature, copper ion concentration and acid concentration), surface area values decreased by decreasing current density and minimum surface area values were obtained at 8.37 A/dm² current density. At the second row for all 3 graphs colored lines showed different temperatures

(20, 30 and 40°C). Likewise, independent of the other parameters surface area values decreased as the temperature increased. The colored lines of the third row figured out different copper ion concentration of the electrolyte (10 and 15 g/L). Free of the other variables, copper powders deposited in the electrolyte containing 15 g/L had smaller surface area than the powders deposited from electrolyte containing 10 g/L. Finally, the effect of acid concentration of the electrolyte on the surface area was plotted at the bottom row. As it could be deduced; whatever the acid concentration of the electrolyte (0.25, 0.5 and 1 M), surface area of the powders was not influenced much with changing acid concentration in the 0.25-1 M acid concentration range. At 0.5 M sulfuric acid concentration, surface area value was at minimum which corresponded to 0.23 m²/g. To sum up, all the parameters except acid concentration had measurable effect on the specific surface area of the electrodeposited copper powders.

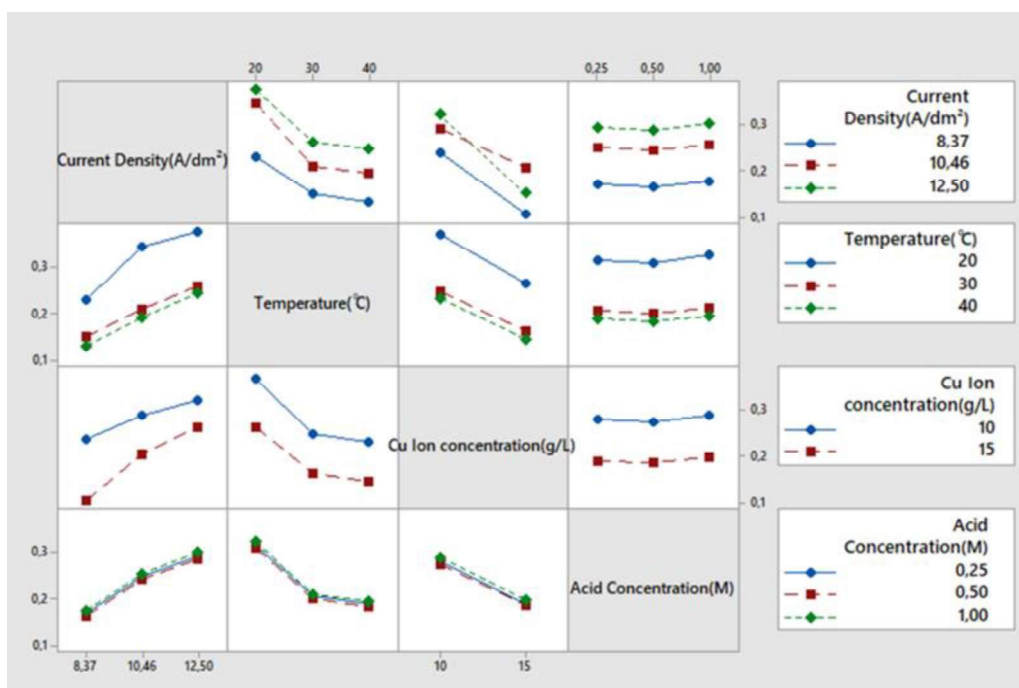


Figure 4.4. Interaction plot for specific surface area of electrodeposited copper powders

The contour plots in mixture design analysis are exhibited in Figure 4.5. The colors on the graphs are based on responses of the two parameters on specific surface area values. Thus, graphs in Figure 4.5, gave combination of the two parameters and revealed minimum surface area values that are shown in the blue area of the charts. According to graphs minimum surface area could be obtained at electrodeposition conditions; 8.37 A/dm², 40°C, 15 g/L copper ion concentration and 0.5 M H₂SO₄ concentration of electrolyte.

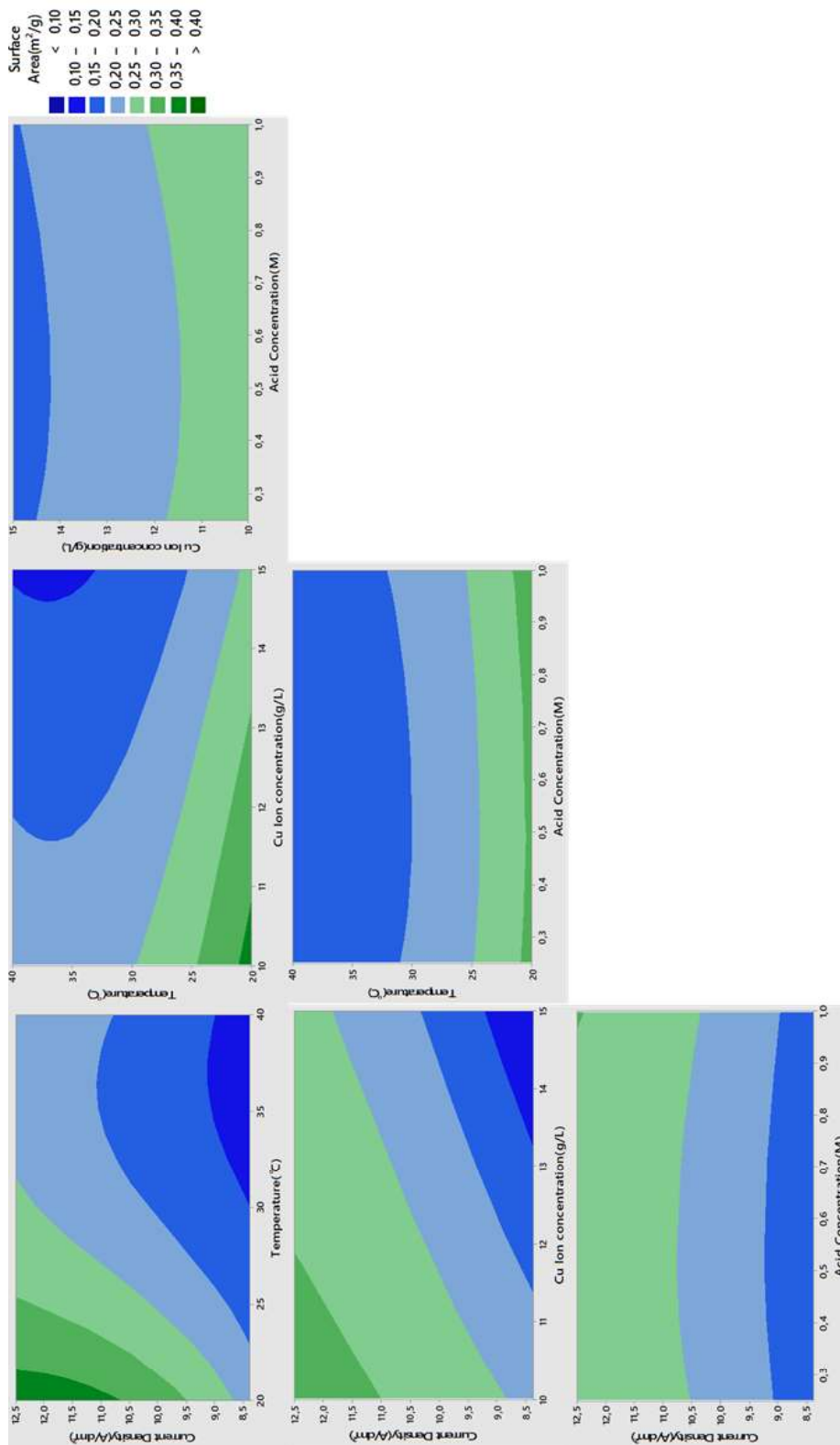


Figure 4.5. Contour plots for specific surface area of electrodeposited copper powder

4.4. Particle Size of Electrodeposited Copper Powder

Mastersizer Hydro 2000S particle size analyzer uses laser diffraction techniques to measure size of particles. The working principle of the particle sizer is that larger angles will be produced when the light scatters from small particles, likewise smaller angles will be scattered from the large particles. It was known that the size of particles in the powder deposit could be changed with the composition, temperature, viscosity and hydrodynamic regime of the electrolyte and the type of deposition regime like galvanostatic or potentiostatic regimes [39]. Powder properties like apparent density, surface area and particle size are interconnected with each other. Figure 4.6 shows the effect of parameters on the particle size of the electrodeposited copper powders.

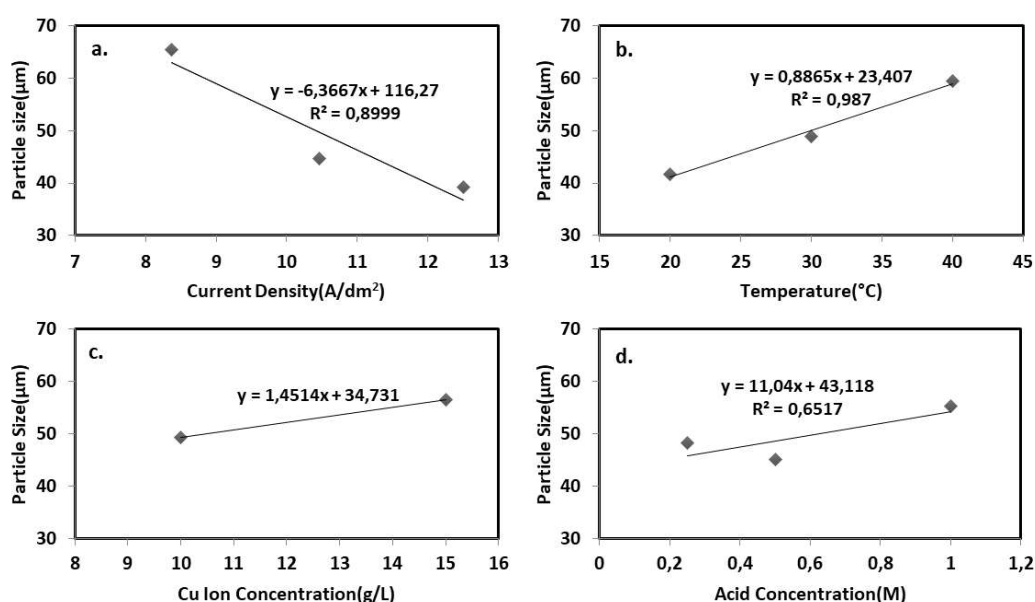


Figure 4.6. Effect of electrolysis parameters on particle size of deposited Cu powder

During analysis it was attained that average size of copper (d₅₀) decreased from 65.1 µm to 41.2 µm while increasing current densities from 8.37 to 12.5 A/dm² as shown in Figure 4.6a. The particle size of electrodeposited copper powders showed linear decreasing dependence with increasing current density. The nucleation rate and hence particle size depended on the current density, therefore particle size of copper decreased a considerable amount at 12.5 A/dm². According to literature, with

increasing current density, the number of growth sites increased and the grain size of the deposit decreased, however, at 8.37 A/dm² current density, deposits grew from a small number of nuclei and grain size increased [40]. By increasing current density, nucleation rate increased, and the hydrogen evolution reaction accelerated, as a result dispersity of powders increased, and particle size decreased. In other words, the particle size variation and applied current density relationship based on the nucleation rate and nuclei growth rate. The nucleation rate was greater than the growth rate at higher current densities, thus electrodeposited copper particle size was finer at 12.5 A/dm² current density [31,39].

By increasing the temperature, diffusion coefficients and metal ion concentration in the electrical double layer near the cathode expanded. At 40°C, an expanded ion source supplied for the cathode, activation energy for the nucleation diminished. Therefore, increasing temperature from 20°C to 40°C caused increasing particle size from 42.1 μm to 59.8 μm as it is seen in Figure 4.6b.

Electrolyte composition had also important effect on the grain size of electrodeposited copper powders. When copper ion concentration increased from 10 g/L to 15 g/L, particle size increased from 48.2 μm to 57 μm according to Figure 4.6c. The particle size strongly affected by the nucleation and growth rate as it was mentioned earlier [42]. When the nucleation rate was much faster than the growth rate of nuclei, more crystal nuclei was formed, and finer particles were obtained as in the case of decreasing copper ion concentration of the electrolyte [43]. Since increase of copper ion concentration accelerated and made easier the formation and growth of nuclei, coarse particle formation was resulted [44]. Likewise, conductivity of electrolyte became higher and electrolyte resistance was reduced by increasing copper ion concentration of the electrolyte. Therefore, overvoltage was decreased, and the cell voltage was reduced while keeping current density constant [45]. Thus, particle size was increased by increasing copper ion concentration.

The effect of acid concentration of electrolyte on the particle size is shown in Figure 4.6d, particle size of copper rapidly decreased from 48.4 to 45.1 when acid concentration was increased from 0.25 M to 0.5 M and then particle size increased to 56.8 when acid concentration was raised to 1M. Raising acid concentration from 0.25M to 0.5M, hydrogen evolution was increased during reduction reaction. Therefore, the diffusion layer thickness was decreased and the particle size was reduced [46]. When acid concentration of electrolyte was further increased to 1M, acid concentration exceeded a certain value and conductivity of the electrolyte became higher and electrolyte resistance was reduced. As explained previously in the case of copper ion concentration, at constant current density, overvoltage and consequently the cell voltage was decreased and particle size was increased [45].

4.5. Specific Surface Area and Particle Size of Cobalt-Copper-Tin Powder

Surface area and particle size were important parameters for powder production, handling and powder processing. While surface area values of collected metallic powders were measured by BET analysis technique in units of m^2/g , particle size measurements were done by Mastersizer Hydro 2000S particle size analyzer. The results are given in terms of average size of metallic powders (d_{50}) in Figure 4.7. Powder numbers given in Figure 4.7 are numbers assigned to electrodeposition conditions as tabulated in Table 4.1.

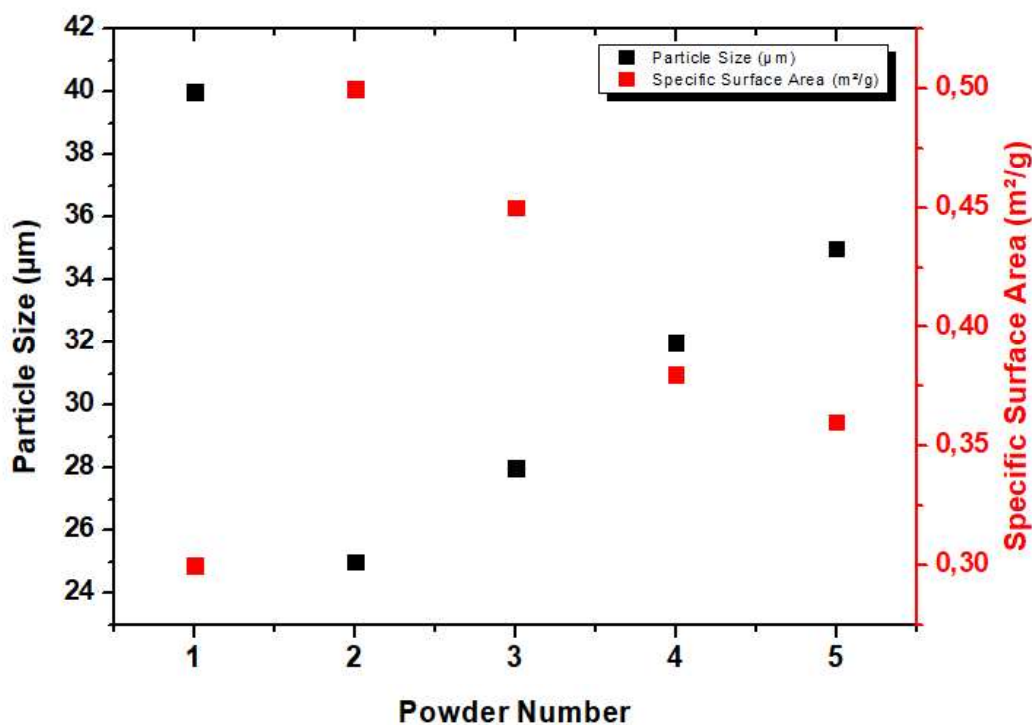


Figure 4.7. Specific surface area and particle size variance of collected metallic powders with respect to electrodeposition conditions

Table 4.1. Powder numbers according to electrodeposition parameters

| Powder Number | Electrodeposition conditions |
|---------------|--|
| 1 | 70 A/dm ² , 30°C, 0.5 M H ₂ SO ₄ , 10 g/L Co ²⁺ |
| 2 | 50 A/dm ² , 30°C, 0.5 M H ₂ SO ₄ , 10 g/L Co ²⁺ |
| 3 | 70 A/dm ² , 40°C, 0.5 M H ₂ SO ₄ , 10 g/L Co ²⁺ |
| 4 | 70 A/dm ² , 30°C, 0.25 M H ₂ SO ₄ , 10 g/L Co ²⁺ |
| 5 | 70 A/dm ² , 30°C, 0.5 M H ₂ SO ₄ , 20 g/L Co ²⁺ |

When powders 1 and 2 are compared, it can be seen that increasing current density decreased specific surface area of powders from 0.52 to 0.31 m²/g. Furthermore, it increased the particle size from 25 µm to 41 µm according to Figure 4.7. As compared to powders produced at 50 A/dm², particles which have smaller specific surface area and larger particle size could be produced at 70 A/dm². As it can be deduced from

particle size and specific surface area graphs, current density has the greatest influence on the electrodeposited cobalt-copper powder when compared to the effects of other parameters. Higher specific area was the result of needle like morphology and massive dendritic structure of metallic powders when compared to compact and smooth surface of cobalt powders and small dendrites of copper powders deposited at high current density.

Comparing metallic powders numbered as 1 and 3, although not as much as the current density, temperature was also an influential parameter in electrodeposited powder properties. Increasing temperature induced decreasing average particle size from 41 to 28 μm and increasing specific surface area from 0.31 to 0.45 m^2/g . Higher temperature reduced the energy required for activation for the nucleation of powders and viscosity of the electrolyte. Therefore, powders deposited at 40°C had lower particle size and higher specific surface area values.

Electrolyte composition should be taken into consideration while determining powder properties in electrodeposition. Decreasing acid concentration as in powder number 4 and increasing cobalt ion concentration as in powder number 5 provoked formation of powders with smaller particle size (32 μm and 35 μm respectively) and larger specific surface area (0.38 m^2/g and 0.35 m^2/g) as compared to powder number 1. Powders deposited at lower acid concentration had smaller particle size and larger surface area because increased electrolyte conductivity promoted the nucleation rate. Increasing cobalt ion concentration made formation and growth of nuclei easier. In addition, formation of hydrogen was reduced by decreasing relative concentration of H^+ ions. Therefore, powders having smaller particle size and larger specific surface area values could be produced by easier nucleation when electrolyte resistance was decreased.

CHAPTER 5

DISCUSSION

Surface area and particle size distributions of the electrodeposited copper powders with respect to changing parameters were shown in previous chapter. In this chapter, results are supported by morphology and x-ray diffraction pattern of the powders.

5.1. Diamond Embedded Copper-Tin Matrix Cutting Tools

5.1.1. Morphology of Electrodeposited Copper Powders

5.1.1.1. Effect of Current Density

Morphology of electrodeposited metallic powders depended on a wide variety of parameters. Current density had a pronounced effect on microstructure and grain size of the electrodeposited copper powders. Also, hydrogen evolution during electrodeposition of metallic powders had significant effect on the morphology and size of the deposited metal powders. It was discussed previously that galvanostatically dispersed metal deposition starts at a current density corresponding to the limiting diffusion current density plateau or higher values [47]. As a second reaction in metal electrodeposition processes, interference of hydrogen evolution reaction at some current density corresponding to the plateau of the limiting diffusion current density. Increasing current density intensifies the hydrogen evolution and outside the plateau of the limiting current density, hydrogen evolution reaction becomes vigorous enough to change the hydrodynamic conditions in the electrolyte near cathode layer.

SEM pictures of powders produced at 8.37 and 10.46 A/dm² current density are shown in Figure 5.1a and Figure 5.1b to compare powders and observe the effect of increasing current density. While coarse and cauliflower like globular copper powders

were formed at current density of 8.37 A/dm^2 , metallic powders were a mixture of dendritic and cauliflower like copper powders at 10.46 A/dm^2 current density.

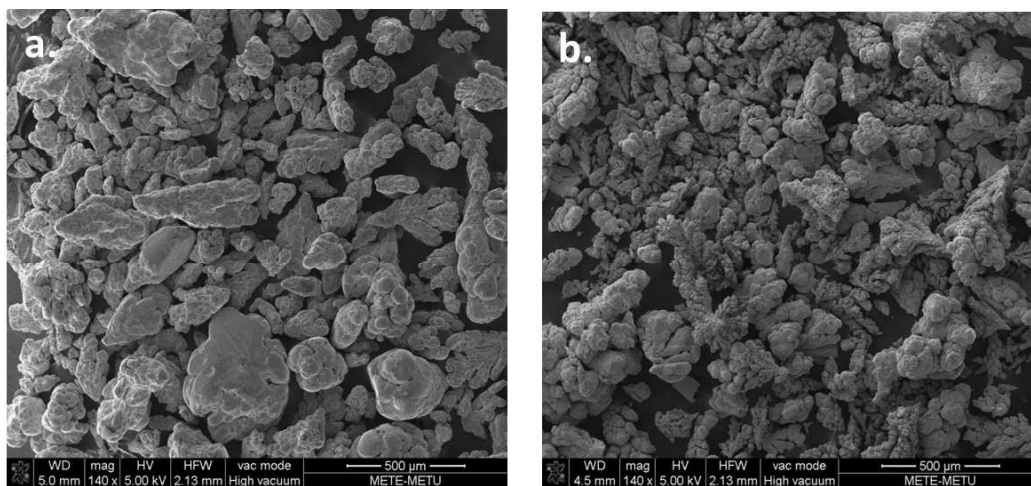


Figure 5.1. SEM pictures of copper deposits obtained at (a) 8.37 A/dm^2 and (b) 10.46 A/dm^2 current density, in 10g/L Cu^{2+} and $0.25 \text{ M H}_2\text{SO}_4$ electrolyte at 30°C

It was obvious that further increase of current density caused formation of acicular dendritic copper powders and finer grain size as imaged in Figure 5.2. This was mainly due to high magnetic field created by high current density. Higher current densities forced ions to hit the cathode and direct reduction of ions took place because of higher applied potential and this caused formation of powders having fine grain size and dendritic shape [25].

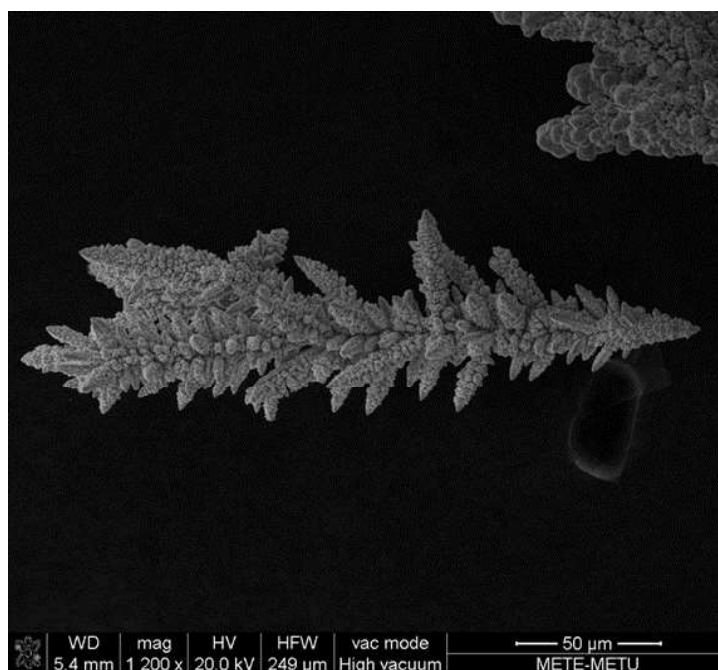


Figure 5.2. SEM picture of copper deposits obtained at 12.5 A/dm^2 current density, in 10g/L Cu^{2+} and $0.25 \text{ M H}_2\text{SO}_4$ electrolyte at 30°C

Increasing current density not only increased the powder deposition rate but it also accelerated hydrogen evolution as explained before. Hydrogen evolution changed the morphology of the electrodeposited copper powder by changing hydrodynamic conditions near the cathode layer. According to Nikolic' et al. [48], if the average current efficiency of hydrogen evolution was higher than or equal to the critical value of 10%, hydrogen evolution was sufficient to change hydrodynamic condition near cathode. Below this critical value, copper powder had dendritic, corn-cob-like morphology and above this value, cauliflower-like powders could be obtained because of dispersity of deposit by hydrogen evolution. From another point of view, in terms of morphology of the electrodeposited copper powder, at high concentration of hydrogen evolution, dispersion of deposit increased during deposition due to hydrogen gas formation [49].

5.1.1.2. Effect of Temperature

Morphology of the electrodeposited copper powder had been influenced strictly by changes of temperature of the electrolyte. As it can be seen from the Figure 5.3, Figure 5.4 and Figure 5.5, microstructure of the powder turned into branched dendrites to compact, globular agglomerates when temperature of the cell was increased from 20°C to 40°C.

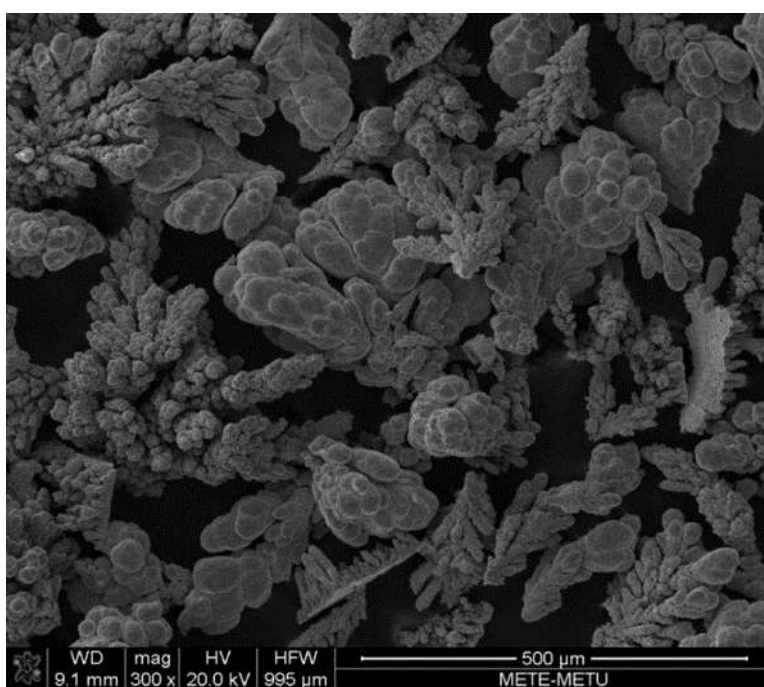


Figure 5.3. SEM picture of copper deposits obtained at 8.37 A/dm² current density, in 10g/L Cu²⁺ and 0.25 M H₂SO₄ electrolyte at 20°C

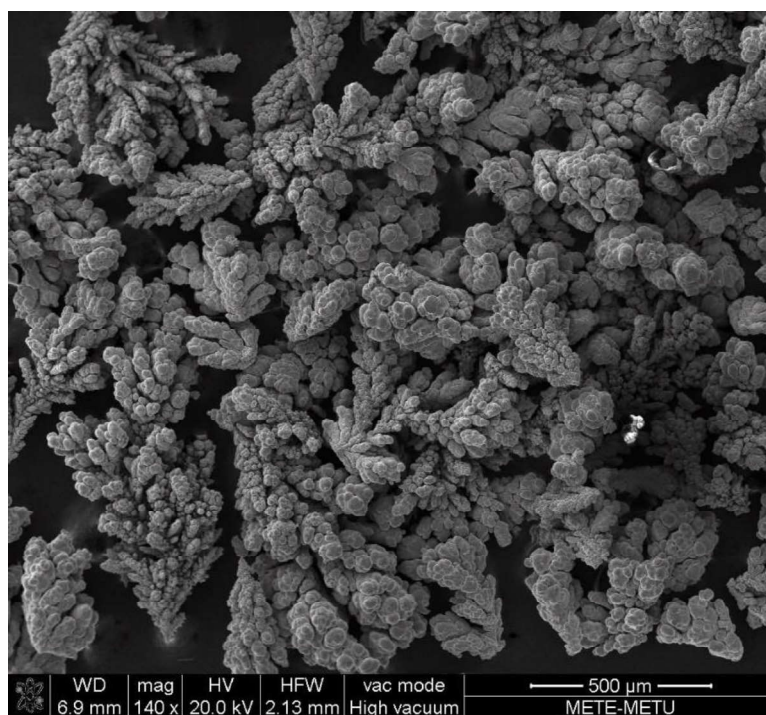


Figure 5.4. SEM picture of copper deposits obtained at 8.37 A/dm² current density, in 10g/L Cu²⁺ and 0.25 M H₂SO₄ electrolyte at 30°C

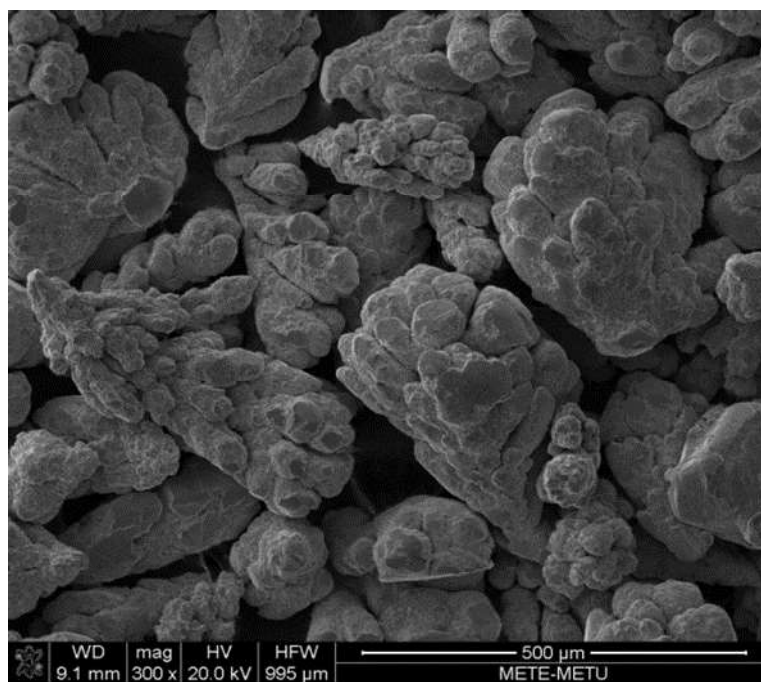


Figure 5.5. SEM picture of copper deposits obtained at 8.37 A/dm² current density, in 10g/L Cu²⁺ and 0.25 M H₂SO₄ electrolyte at 40°C

These observations could be easily explained in terms of increasing fluidity of the electrolyte in which easier movement of the ions throughout the electrolyte takes place. Increase in diffusivity could also be accounted. When accelerated ions reach immediately to the stainless steel cathode surface and they agitate the concentration layer, thus concentration polarization and accordingly the cell voltage decreases [50]. Therefore, at high operating temperatures, compact and denser copper powders were obtained. In addition, increasing electrolyte temperature increased the current efficiency of the process by reducing hydrogen evolution and consequently decreased the energy demand to produce Cu powder [51]. But it was important to catch the critical hydrogen evolution percentage to optimize the morphology of powder according to intended use.

These morphological changes were assigned to reducing concentration polarization by easy diffusion of more mobile ions in electrolyte at higher temperatures. Therefore, it gave rise to increasing powder deposition rate and growth of equiaxed grains on the cathode surface.

5.1.1.3. Effect of Electrolyte Composition

CuSO_4 and H_2SO_4 were the main constituents of the electrolyte. In electrodeposition, while the source of reduced ions at the cathode was anode itself and $\text{CuSO}_4 \cdot 5\text{H}_2\text{O}$ salt, the main component determining the degree of conductivity of the electrolyte was the sulfuric acid concentration. Compact and more dense copper powders obtained by increasing cupric ion concentration of the electrolyte as compared in Figure 5.6a and Figure 5.6b where CuSO_4 concentration was increased from 10 g/L to 15 g/L.

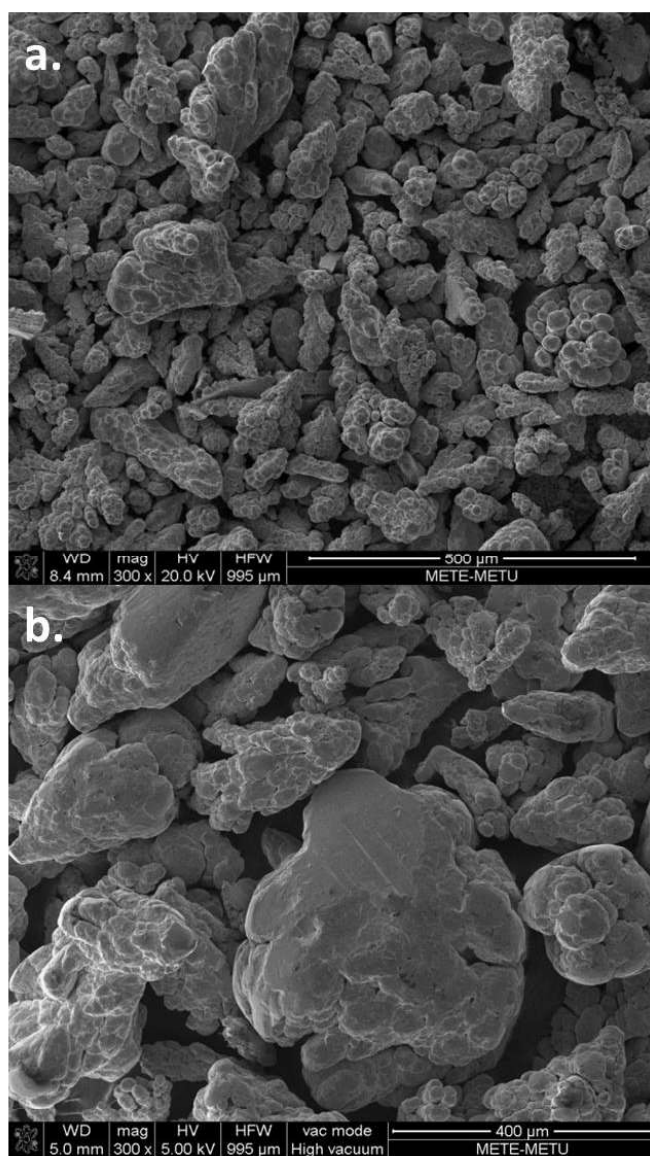


Figure 5.6. SEM pictures of copper deposits obtained in (a) 10g/L Cu^{2+} and (b) 15g/L Cu^{2+} , at 10.46 A/dm^2 current density, in 0.5 M H_2SO_4 electrolyte, at 30°C

High concentration of copper ions caused decrease in cathodic polarization and overvoltage near cathode surface mainly due to more copper ions present near cathode surface during deposition. Adequate and constant feed of Cu^{2+} ions to the cathode surface induced decrease of concentration polarization and H_2 overvoltage [50,51]. By constant feed of copper ions, deposition rate and growth of sidelong branches increased and as a result compact, dense and large grain size powders were deposited

as it can be seen from SEM images of powders (Figure 5.6) obtained at two different Cu ion compositions of electrolyte.

But it was critical to think that when concentration of Cu^{2+} ions increased in the solution, ability of solution stirring by evolved hydrogen declined due to the decrease of relative concentration of H^+ ions according to Figure 5.7 [54]. Therefore, concentration of electrolyte was carefully adjusted so that evolved hydrogen was high enough to change hydrodynamic conditions, but hydrogen evolution should be optimized to yield desired properties of collected copper powders.

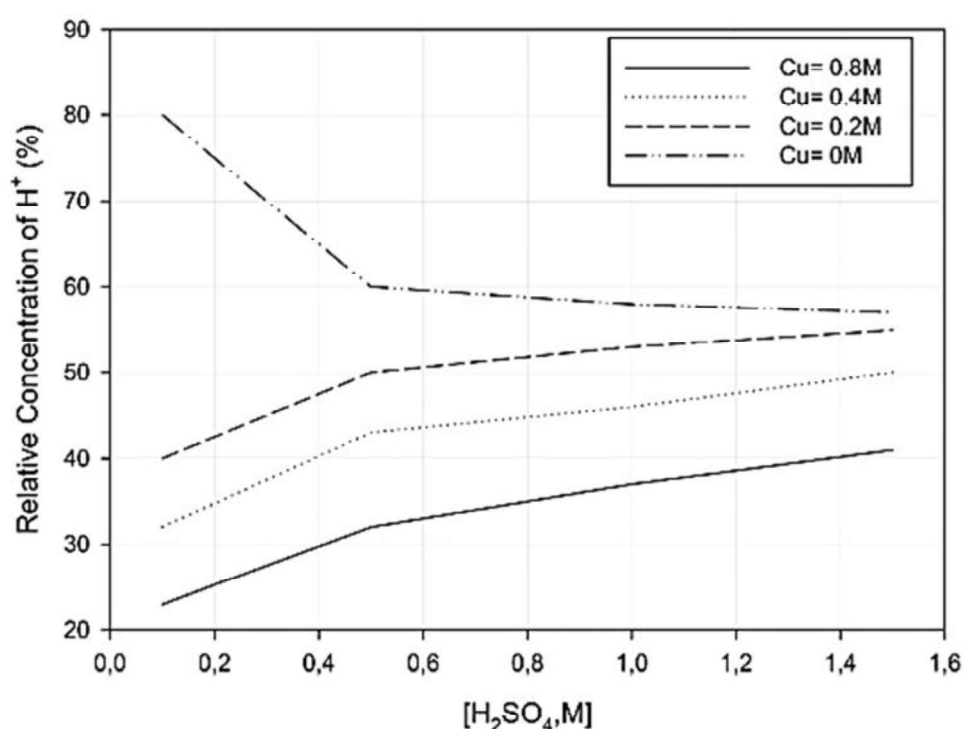


Figure 5.7. Relative concentration of hydrogen ions as a function of sulfuric acid and total copper concentrations, at 25°C [54]

As H^+ ion concentration was increased with increasing H_2SO_4 concentration in the electrolyte, hydrogen evolution reaction became faster due to increased current efficiency of hydrogen evolution. Hydrogen evolution changed the morphology of the electrodeposited powder as could be deduced from SEM images of electrodeposited copper powders at two different sulfuric acid concentrations of electrolyte as shown

in Figure 5.8. According to Figure 5.8a and Figure 5.8b, changing acid concentration from 0.25 M to 1 M shows small effect on morphology of the copper powders. As it is shown, copper powders electrodeposited in 0.25 M sulfuric acid concentration are more packed than those obtained in 1 M sulfuric acid concentration electrolyte and these powders have tree-like morphology.

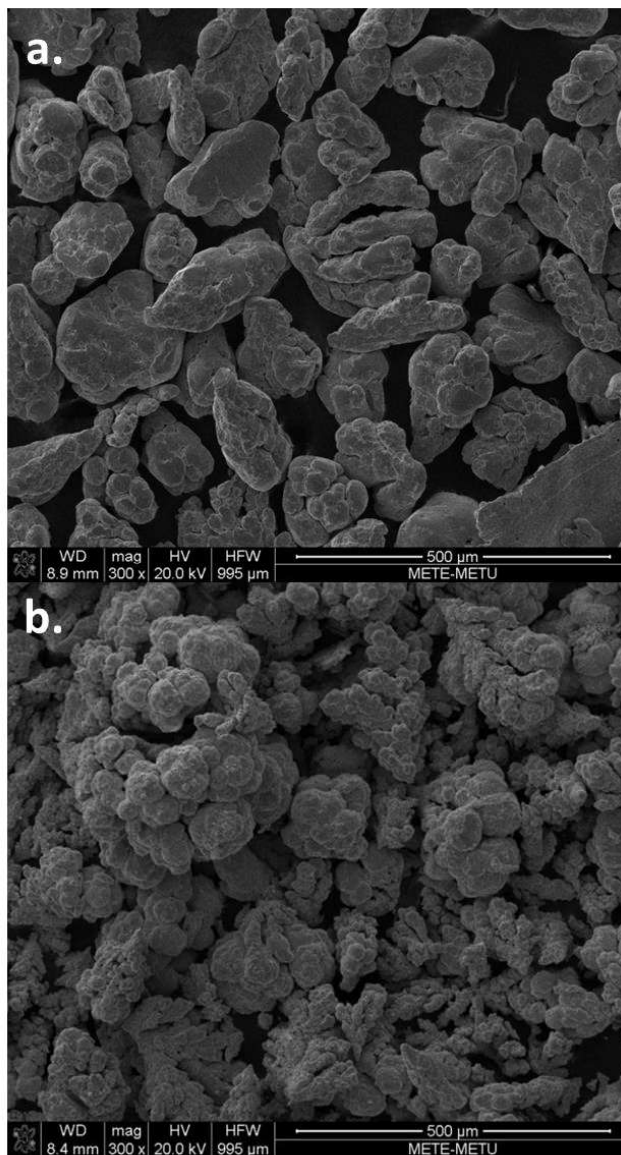


Figure 5.8. SEM pictures of copper deposits obtained in (a) 0.25 M and (b) 1 M H₂SO₄ at 10.46 A/dm² current density, in 15g/L Cu²⁺ electrolyte at 30°C

5.1.2. Crystallography of Electrodeposited Copper Powders

X-ray diffraction could be explained as; high energy incident beams of X-ray interfered with each other as they leave the crystal mainly due to atomic plane of a crystal. Thus, diffraction patterns of powders show intensities of diffractions from atomic planes. The highest intensity of diffraction comes from the most densely packed plane and the others aligned in accord with their diffraction angles. However, this order changes when the growth is affected by electroplating conditions to reveal growth orientations. X-Ray diffraction patterns of copper powders were examined to see how electrodeposition parameters affected crystallographic orientations of the powders from the following Figure 5.10, Figure 5.11 and Figure 5.12 comparatively.

Apart from different parameters, Rietveld refinements were done for all collected powders by using Maud to get information on microstructural characteristics of samples. Maud was an advanced Rietveld software, since quantitative analysis and crystal structure analysis were performed. An example of the Rietveld analysis is shown in Figure 5.9. After final Rietveld refinement, Rexp value decreased to 10.47 %, which means that good fitting was done. The peak positions of copper powder sample were located at 2θ angles of 43.31, 50.44, 74.12 and 89.93 degrees. The peak positions and intensity ratios matched the corresponding (111), (200), (220) and (311) reflections related to the face centered cubic copper phase. However, the peak positions of copper oxide were located at 2θ angles of 29.98, 37.0 and 42.61 degrees which were well corresponded to (110), (111) and (200) reflections of Cu_2O phase. According to analysis result, some of the copper powders were oxidized and approximately 87.75 ± 1.83 wt% of collected powders were copper having 3.6135 \AA lattice constant and FCC crystal structure, while other 12.25 ± 1.62 wt% of powders were copper oxide (Cu_2O) having 4.2666 \AA lattice constant and cubic structure. These findings were good agreement with literature [53,54].

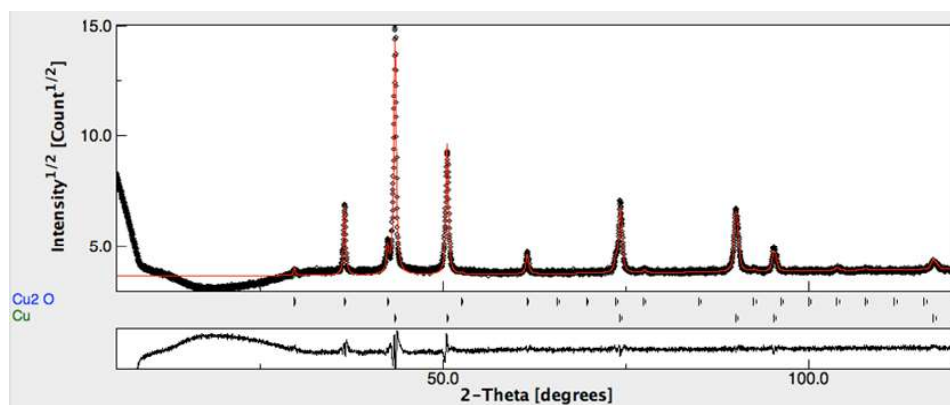


Figure 5.9. Rietveld analysis of electrodeposited copper powders by using Maud software

Diffraction patterns of copper powders produced at constant 12.5 A/dm^2 current density and 10 g/L constant copper ion concentration of electrolyte with different temperature and acid concentrations are illustrated in Figure 5.10. As it can be deduced; increasing temperature from 20°C to 40°C , intensity of the peaks of copper powders decreased relatively. Also, increasing sulfuric acid concentration of electrolyte from 0.25 M to 1 M had minor effect on intensity of the diffractions of the copper powders. Intensity of diffractions from (111) plane of produced copper was mostly dominated when copper powders were deposited at 20°C and $1 \text{ M H}_2\text{SO}_4$ concentration. The growth texture of copper deposits mostly oriented to the indicated direction under above mentioned conditions. This orientation was supported by SEM images (see Figure 5.3, Figure 5.5 and Figure 5.8) which meant that decreasing temperature and increasing sulfuric acid concentration of electrolyte caused producing more dendritic copper powders that mostly grow in one direction. These diffraction patterns and morphology of the electrodeposited copper powders supported each other.

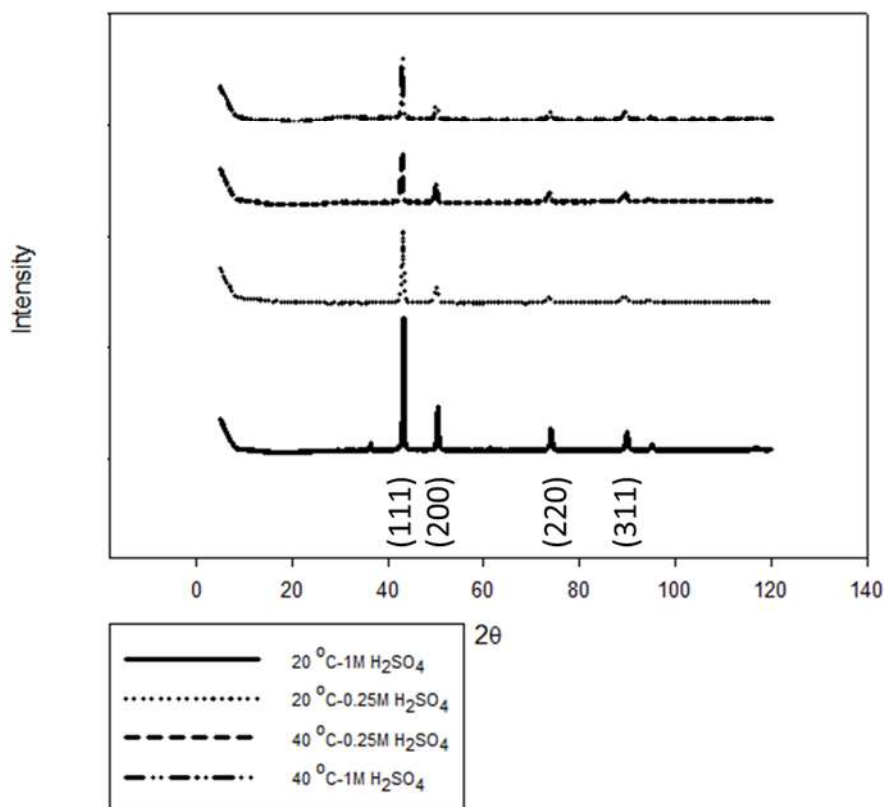


Figure 5.10. XRD patterns of electrodeposited copper powders produced at constant 12.5 A/dm² current density and 10 g/L constant copper ion concentration of electrolyte with two temperature and acid concentration of electrolyte

To make comparison between diffraction patterns of copper powders deposited under two different acid concentrations of electrolyte and at two different current densities are shown in Figure 5.11 at constant 15 g/L copper ion concentration at 40°C constant temperature. When current density was increased from 8.37 A/dm² to 12.5 A/dm², density of the (111) plane which was most densely packed plane of copper decreased. Therefore, orientation was enhanced, and formation of oriented, dendritic copper powders actualized as could be seen from SEM images (see Figure 5.1, Figure 5.2 and Figure 5.8).

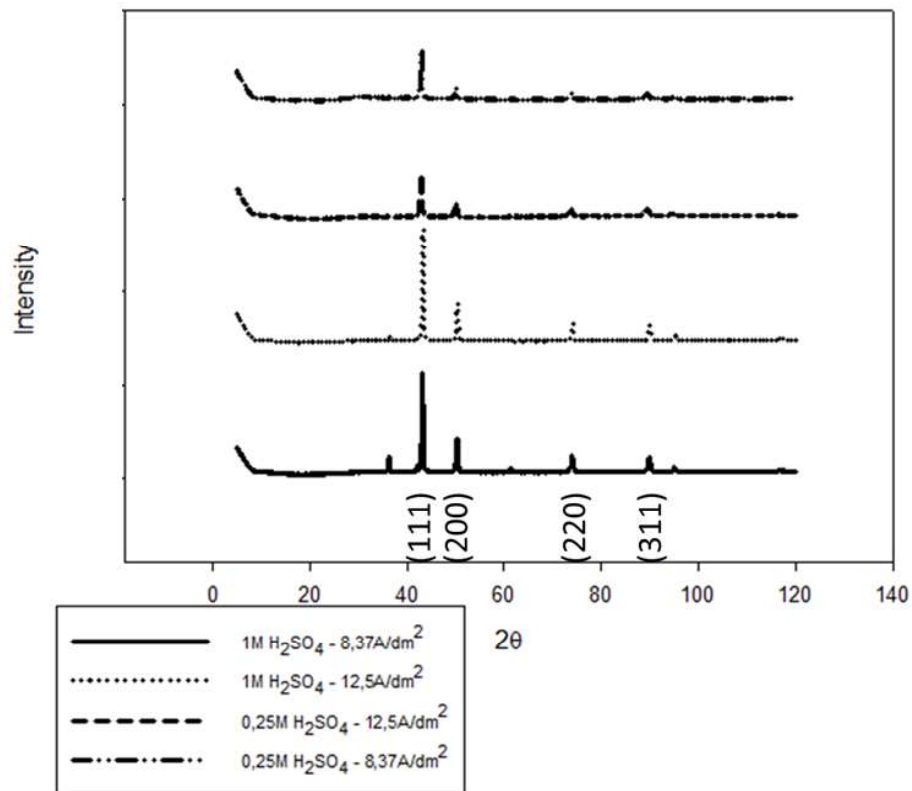


Figure 5.11. XRD patterns of electrodeposited copper powders produced at constant 15 g/L copper ion concentration at 40°C constant temperature with two different current density and acid concentration of electrolyte

Likewise, increasing copper ion concentration of electrolyte and decreasing current density caused production of globular, compact powders as shown in SEM images (see Figure 5.1, Figure 5.2 and Figure 5.6) which was verified by X-Ray diffraction patterns in Figure 5.12. This figure showed X-Ray diffraction patterns of copper powders electrodeposited at constant 1 M sulfuric acid concentration at 40°C constant temperature. At higher current density and low copper ion concentration, (111) plane growth prompted therefore dendritic and acicular copper powders were produced accordingly.

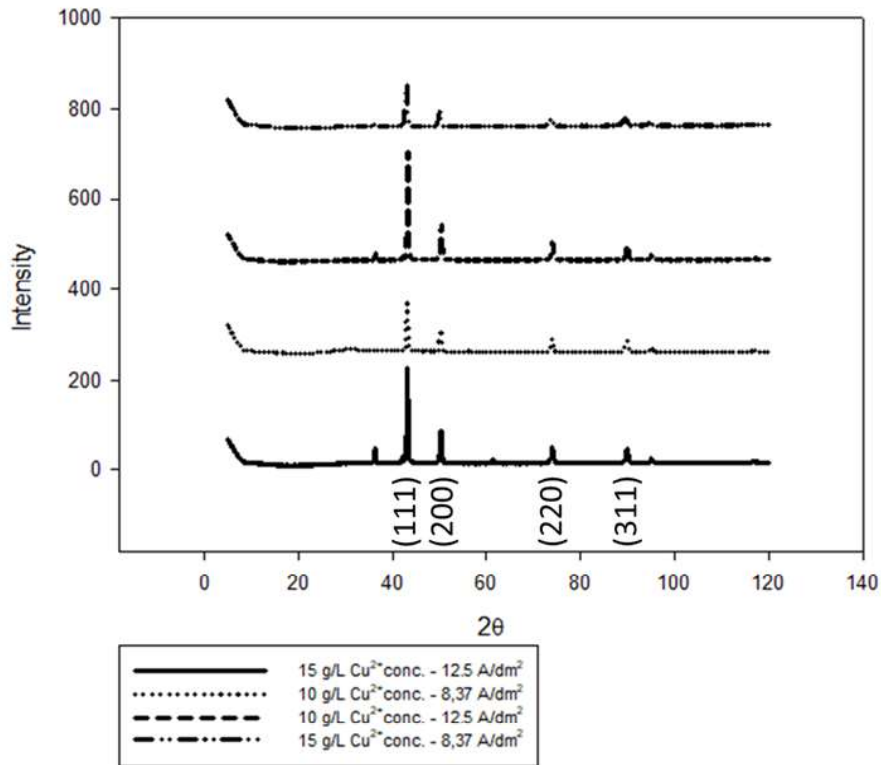


Figure 5.12. XRD patterns of electrodeposited copper powders produced at constant 1M acid concentration of electrolyte and 40°C constant temperature with two different current density and copper ion concentration of electrolyte

5.2. Diamond Embedded Cobalt-Copper-Tin Matrix Cutting Tools

5.2.1. Morphology of the Electrodeposited Cobalt-Copper-Tin Powders

Morphology of the electrodeposited metal powders was strongly dependent on the deposition condition as proved in the recovery of diamond embedded copper-tin matrix cutting tools. As in the case of copper-tin matrix composite cutting tools, diamond particles were separated from the matrix while other metal constituents dissolved from the anode. Diamond particles sunk to the bottom of electrolyte and they were filtered after the experiments. In this situation, because of high current densities, tin powders were also collected from the cathode which means potential created by the applied current density was high enough for oxidation reactions of cobalt, copper and tin.

5.2.1.1. Effect of Current Density

Current density is an important parameter that affects the morphology of the metal powders. In Figure 5.13a and Figure 5.14a, SEM images of metal powders that were deposited at 50 A/dm^2 and 70 A/dm^2 are shown respectively. While metallic powders numbered as 1 in both figures shows copper powders, cobalt powders are numbered as 2 and tin powders are numbered as 3. With respect to copper powders, morphology is generally almost the same dendritic structure for two different current density values. However, the size and shape of dendrites were quite different in which copper powders obtained at high current density (Figure 5.14a) caused formation of small dendrites. While copper powders deposited at 50 A/dm^2 had massive dendritic structure with secondary branches, copper powders deposited at 70 A/dm^2 composed of batch of dendrites with a numerous small branch. The result of dendritic shape of the copper powders in both images was mainly due to the large excess current densities relative to the limiting current density. High magnetic field caused direct reduction of the copper powders and due to serious hydrogen evolution, copper powders were formed in dendritic shape. From these two SEM images, no characteristic structure of uniform tin powders distributed homogenously between others can also be seen. The contrast of tin powders can be distinguished due to charging from the surface.

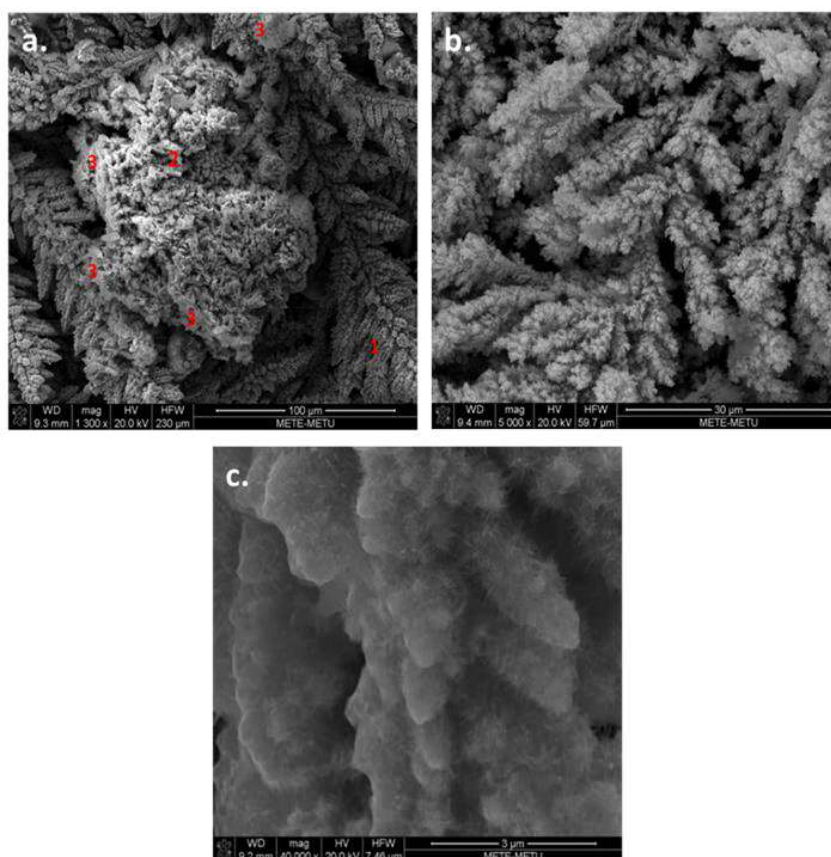


Figure 5.13. SEM pictures of (a) cobalt-copper-tin, (b) and (c) cobalt deposits obtained at 50 A/dm² current density, in 10 g/L Co²⁺ and 0.5 M H₂SO₄ electrolyte at 30°C

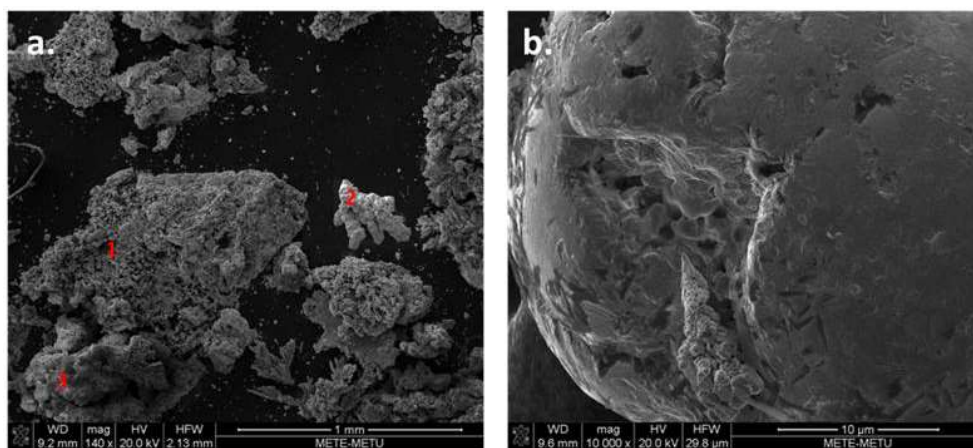


Figure 5.14. SEM pictures of (a) cobalt-copper-tin and (b) cobalt deposits obtained at 70 A/dm² current density, in 10 g/L Co²⁺ and 0.5 M H₂SO₄ electrolyte at 30°C

Increasing current density caused changes in the morphology of cobalt powders and produced regular, compact agglomerates with deep cavities. The morphologies of Co powders formed at two current densities are compared in Figure 5.13b, Figure 5.13c

and Figure 5.14b. The observed cobalt powder structure was dendritic when it was deposited at a 50 A/dm^2 current density which almost corresponds to limiting current density for cobalt electrodeposition. The cobalt dendrites had fern-like structure comprised of the small needle like protrusions as shown in Figure 5.13c. However cobalt powders deposited at 70 A/dm^2 current density, had cauliflower like agglomerates with deep cavities on the surface. The cobalt grains around holes had smooth and regular surface with some nanopores as shown in Figure 5.14b. These nano-pores were formed mainly due to detachment of hydrogen bubbles which was the result of vigorous hydrogen evolution during the deposition of cobalt particles at higher current density values.

As a secondary reaction during cobalt electrodeposition, hydrogen evolution had played an important role on the morphology of the deposited powders. In the case of dendritic powder formations, evolved hydrogen prevented the growth of the dendrites in the side directions inducing vertically dominant growth as shown in Figure 5.13. The powder deposition started by formation of a nucleus and following growth of dendritic particle took shape according to hydrogen evolution. As already mentioned, hydrogen evolution reaction accelerated by increasing current density and vigorous hydrogen evolution prevents dendritic growth. Decreased thickness of diffusion layer was the result of effective stirring of the electrolyte near electrode layer by enough hydrogen evolution. In addition, vigorous hydrogen evolution caused increase in limiting current density and decrease in the degree of diffusion control of electrodeposition process [57]. Therefore, formation compact agglomerates at 70 A/dm^2 proved that the degree of diffusion control was lower during deposition of cobalt powder at 70 A/dm^2 than at 50 A/dm^2 due to accelerated hydrogen evolution reaction. Also, hydrogen played two important roles in the electrodeposition process. One of the roles was creation of pores and holes which influenced the overall specific surface area of the compact agglomerates. The remaining part of hydrogen was responsible for adjusting hydrodynamic conditions in the near electrode layer by stirring the electrolyte [58].

5.2.1.2. Effect of Temperature

Temperature is also an important parameter for the morphology of the metal powders as discussed earlier and it was derived from copper matrix cutting tools recycling studies that increasing temperature caused formation of compact and regular copper powders. To see the effect of temperature on morphology in the case of Co-Cu-Sn matrix waste cutting tools, metal powders deposited at 30°C and 40°C are shown in Figure 5.14a and Figure 5.15a respectively. Like previous images, copper powders were labeled as 1, cobalt powders as 2 and tin powders as 3. Copper powders obtained at 30 and 40°C were dendritic in shape in both SEM images and they resembled each other because, at these current densities, morphology of the copper powder was all dendritic as previously explained. Tin powders also had indistinct structure with uniform distribution. The effect of temperature had pronounced effect on the cobalt powders as could be followed from SEM images represented in Figure 5.14b and Figure 5.15b. With increasing temperature morphology of the cobalt powders turned from smooth, regular powders with deep holes to needle like structure on dendritic protrusions.

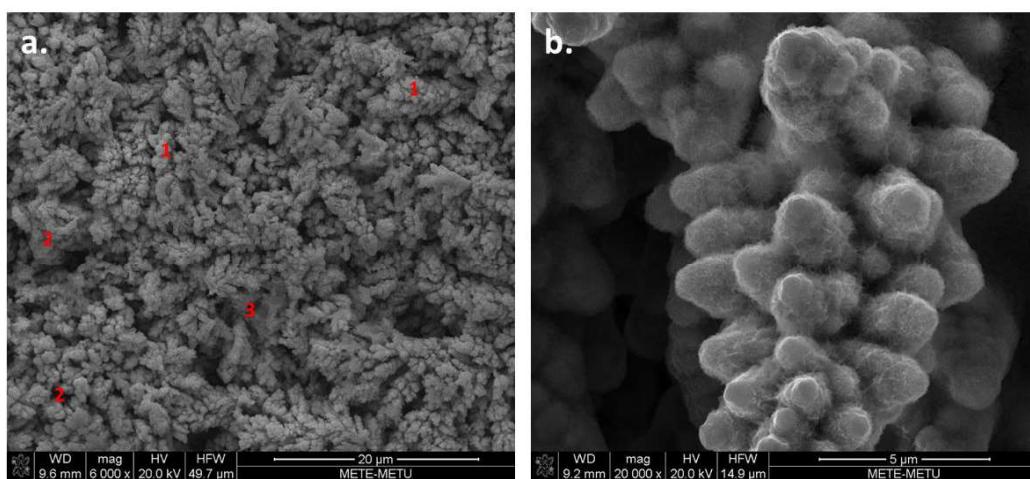


Figure 5.15. SEM pictures of (a) cobalt-copper-tin and (b) cobalt deposits obtained at 70 A/dm² current density, in 10 g/L Co²⁺ and 0.5 M H₂SO₄ electrolyte at 40°C

SEM image of cobalt powders shown in the Figure 5.15a was reproduced at higher magnification and shown in Figure 5.15b for better examination of the cobalt

structure. As it can be seen cobalt had needle-like morphology when temperature was increased to 40°C.

Diffusion coefficients are in general temperature dependent, therefore increasing temperature facilitated the movement of cobalt ions through electrolyte. Concentration polarization decreased by easy movement of ions near to the electrode layer, therefore constant and sufficient feed of cobalt ions for deposition was provided. Thus, increasing electrolyte temperature caused decreasing current efficiency for hydrogen evolution and consequently hydrogen evolution was reduced. Therefore, at lower temperatures, hydrogen evolution was sufficient to prevent formation of dendritic powders and cavities and deep holes on the surface of cobalt powders formed due to hydrogen bubbles attachment. Additionally, insufficient hydrogen evolution facilitated formation of dendritic powders at higher temperatures (40°C).

5.2.1.3. Effect of Electrolyte Composition

Another important parameter for electrodeposition to control morphology of the deposited metallic powders is the electrolyte composition. For the recovery of diamond embedded cobalt-copper-tin matrix cutting tools, electrolyte was mainly composed of sulfuric acid and a cobalt sulfate salt. Effect of cobalt ion concentration on the morphology of cobalt powders were studied by changing Co^{2+} concentration 10 g/L and 20 g/L. Morphology of the metallic powders obtained at these compositions are given in Figure 5.14a and Figure 5.16a respectively. The same designations; 1, 2 and 3 were used for copper, cobalt and tin metallic powders in both figures. As it could be deduced, the only copper source for electrodeposition of copper powders was the anode itself. Therefore, there was no difference in collected copper and tin powders in terms of bath composition. The morphology of copper powders was dendritic in shape and similar sizes and structure. The effect of Co^{2+} ion concentration on cobalt morphology can be seen from cobalt powders which was labeled as 2 in Figure 5.16a, were magnified in Figure 5.16b and Figure 5.16c for closer examination.

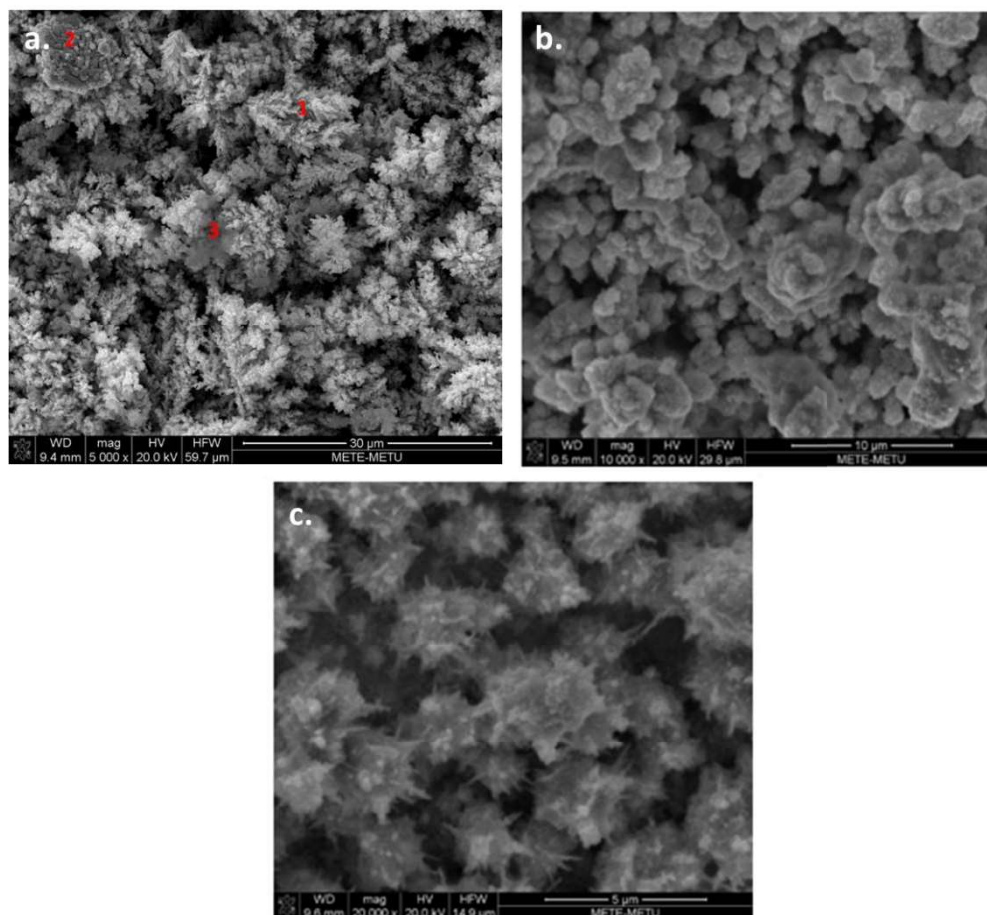


Figure 5.16. SEM pictures of (a) cobalt-copper-tin, (b) and (c) cobalt deposits obtained at 70 A/dm² current density, in 20 g/L Co²⁺ and 0.5 M H₂SO₄ electrolyte at 30°C

At higher magnifications, cobalt powders showed lamellar structure, which means cobalt powders deposited layer by layer (Figure 5.16b). By further increased magnifications, these layers comprised of number of protrusions with needle like morphologies as shown in Figure 5.16c. More and more cobalt ions near the cathode layer decreased the cathodic polarization and overvoltage near the cathode as mentioned in recovery of diamond embedded copper-tin matrix cutting tools part. Therefore, concentration polarization and overpotential of hydrogen evolution decreased which means quantity of the evolved hydrogen decreased. When increasing cobalt ion concentration of electrolyte from 10 g/L to 20g/L, relative concentration of H⁺ ion and consequently quantity of evolved hydrogen decreased. As a result, the

ability of solution stirring deteriorated. As it can be seen from the SEM image in Figure 5.16b and Figure 5.16c, the quantity of evolved hydrogen prevented the growth of dendrite towards side directions. Also, due to nucleation and growth phenomena, at the first stage, existing cobalt ions in the solution started to deposit on the cathode surface and formed protrusions on the surface. As time progressed, while protrusions grew under activation or mixed control, deposition to the flat part of the electrode surface was under complete diffusion control [59]. Therefore, as time progressed cobalt ion concentration was nearly diminished at the flat part of the cathode which was the result of the formation of dendritic and needle-like cobalt powders. However, cobalt powders deposited from electrolyte containing 10 g/L cobalt ion, in which more hydrogen gas evolution occurred, evolved hydrogen promoted both solution stirring and formation of cavities and holes by attaching the surface of cobalt powders at cathode as could be seen in Figure 5.14b.

Effect of sulfuric acid concentration had dramatic effect on the microstructure of the cobalt powders contrary to deposition of copper powders explained earlier. Metallic powders obtained from electrolyte containing 0.25 M and 0.5 M sulfuric acid concentration are illustrated in Figure 5.17a and Figure 5.14a. The morphologies of copper and tin powders were not affected much by the acid concentrations of the electrolyte (0.25 M and 0.5 M). However, cobalt powders had quite different structures when deposited from the electrolyte containing 0.25 M and 0.5 M sulfuric acid. Cobalt powders deposited in electrolyte having 0.5 M acid concentration, shown in Figure 5.14b, had smooth surface with irregular holes as already mentioned. On the contrary, cobalt powders deposited in electrolyte having 0.25 M acid concentration, had quite different morphology as shown in the Figure 5.17b.

Cobalt powders deposited from electrolyte containing 0.25 M sulfuric acid had thorny structure as illustrated in Figure 5.17b. Lower acid concentration meant lower H^+ ion concentration and less amount of evolved hydrogen. Therefore, formation of thorny structure was due to less quantity of evolved hydrogen causing inadequate stirring of the electrolyte and lower conductivity of the electrolyte.

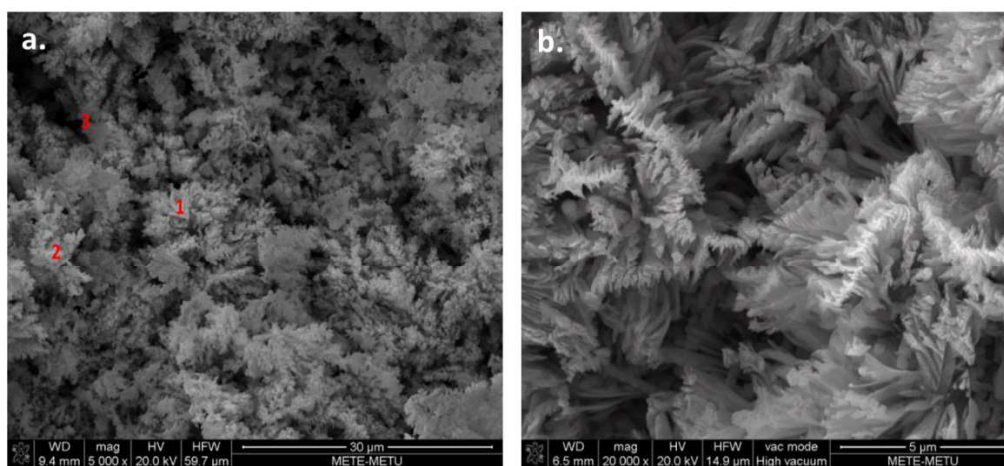


Figure 5.17. SEM pictures of (a) cobalt-copper-tin and (b) cobalt deposits obtained at 70 A/dm² current density, in 10 g/L Co²⁺ and 0.25 M H₂SO₄ electrolyte at 30°C

5.2.2. Crystallography of Electrodeposited Metallic Powders

To determine crystallinity and phase distribution of the collected powders XRD analyses were performed. Then Rietveld analysis was applied to diffraction patterns of the collected metallic powders by Maud program to confirm crystal structure and quantitative analysis. After several Rietveld refinements, R_{exp} value decreased to nearly 14.72 %, which was proof of the good fit. It was derived from the Rietveld analysis of metallic powders obtained at 70 A/dm² current density, from electrolyte which contained 0.5 M sulfuric acid and 10 g/L cobalt ion at 30°C as shown in Figure 5.18. Collected powders comprised of 3% tin, 15% copper and 82% cobalt having hexagonal-close pack structure (hcp) at these electrodeposition conditions. However, Rietveld analysis of metallic powders obtained at 70 A/dm² current density, from electrolyte which contained 0.5 M sulfuric acid and 20 g/L cobalt ion at 30°C as shown in Figure 5.19 was different. As it can be deduced from the analyses, increasing cobalt ion concentration of electrolyte caused formation of some of the metallic cobalt in face centered cubic structure (fcc). Collected powder composition was 2% tin, 16% copper, 5% cobalt of fcc structure and 77% cobalt of hcp structure.

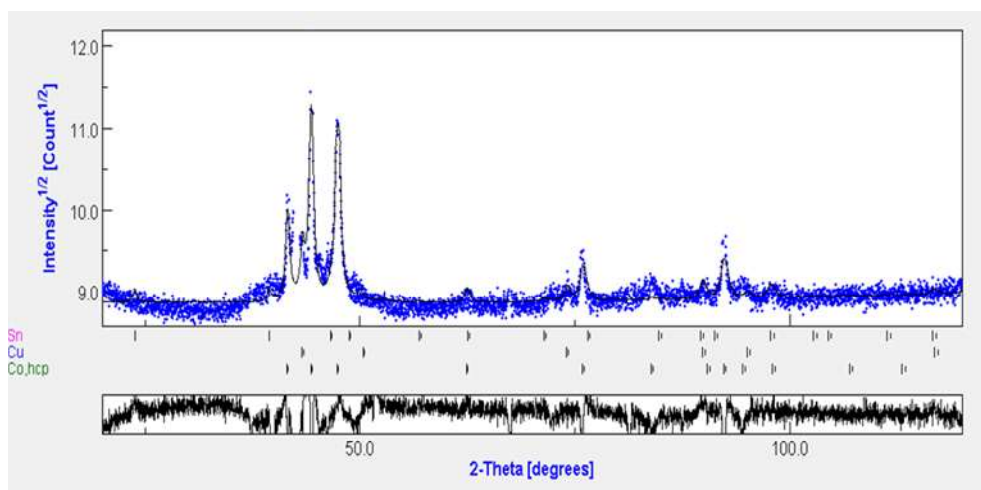


Figure 5.18. Rietveld analysis of electrodeposited cobalt-copper-tin powders at 70 A/dm² current density, in 10 g/L Co²⁺ and 0.5 M H₂SO₄ electrolyte at 30°C by Maud program

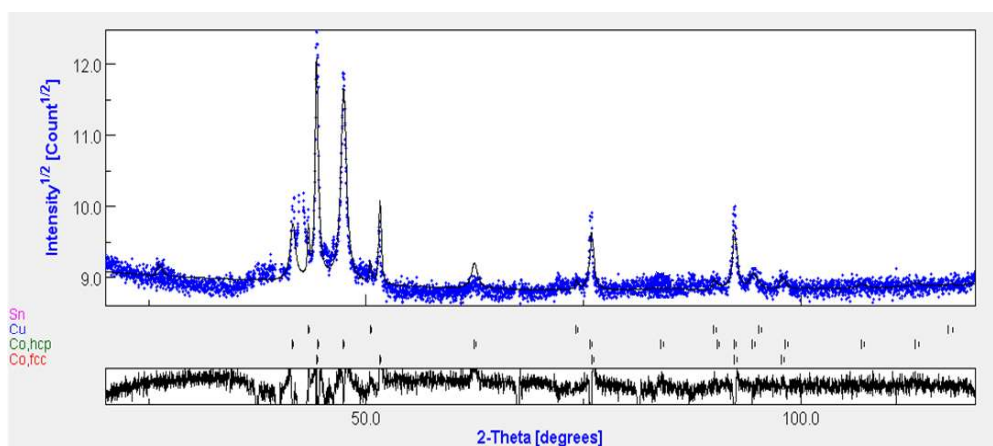


Figure 5.19. Rietveld analysis of electrodeposited cobalt-copper-tin powders at 70 A/dm² current density, in 20 g/L Co²⁺ and 0.5 M H₂SO₄ electrolyte at 30°C by Maud program

Compositions of electrodeposited metallic powders at different electrodeposition conditions are tabulated in Table 5.1. According to table, parameters had different effects on the quantity of the cobalt powders having fcc structure.

Table 5.1. Compositions of electrodeposited metallic powders

| Electrodeposition conditions | Tin (wt%) | Copper (wt%) | Cobalt (hcp)(wt%) | Cobalt (fcc)(wt%) |
|--|-----------|--------------|-------------------|-------------------|
| 70 A/dm ² , 30°C, 0.5 M H ₂ SO ₄ , 10 g/L Co ²⁺ | 3 | 15 | 82 | - |
| 50 A/dm ² , 30°C, 0.5 M H ₂ SO ₄ , 10 g/L Co ²⁺ | 3 | 15 | 70 | 12 |
| 70 A/dm ² , 40°C, 0.5 M H ₂ SO ₄ , 10 g/L Co ²⁺ | 2 | 16 | 72 | 10 |
| 70 A/dm ² , 30°C, 0.25 M H ₂ SO ₄ , 10 g/L Co ²⁺ | 3 | 17 | 73 | 7 |
| 70 A/dm ² , 30°C, 0.5 M H ₂ SO ₄ , 20 g/L Co ²⁺ | 2 | 16 | 77 | 5 |

To see the differences between diffraction patterns of the metallic powders analyzed in Figure 5.18 and Figure 5.19 in detail, XRD patterns of these powders obtained at two different conditions are drawn in Figure 5.20 between 2θ values of 20° and 60°.

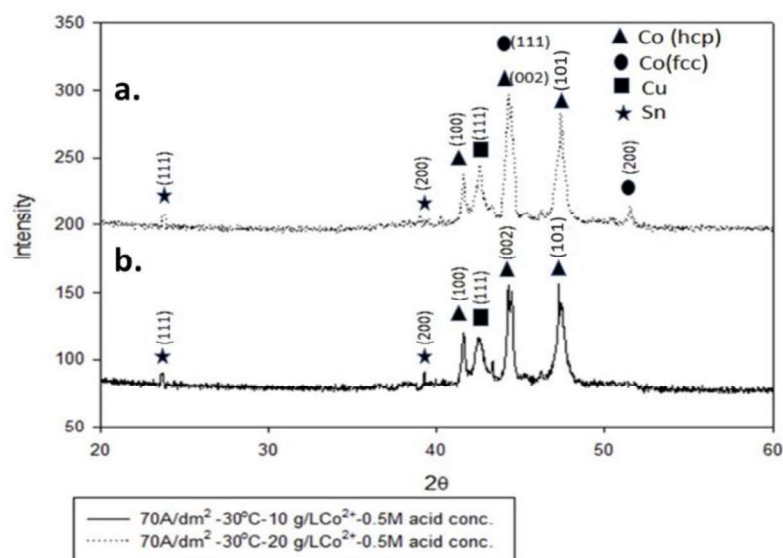


Figure 5.20. X-Ray diffraction patterns of electrodeposited metallic powders in (a) 20 g/L Co^{2+} and (b) 10 g/L Co^{2+} , 0.5 M H_2SO_4 electrolyte at 70 A/dm² current density, at 30°C

The diffraction at 2θ values 43.30 was (111) reflections of copper phase, and 23.69 and 39.24 were corresponding to 2θ values of (111) and (200) reflections of alpha tin phase [60]. The peak positions of cobalt powders were positioned at 2θ angles 41.68°, 44.76° and 47.76°. The peak positions and intensities are in good agreement with the corresponding (100), (002) and (101) reflections of hcp cobalt phase (JCPDS: 05-0727) [60]. The XRD patterns in Figure 5.20 are obtained from the metallic powders electrodeposited at 70 A/dm² current density, 30°C, from electrolyte which contained 0.5 M sulfuric acid, 10 g/L and 20 g/L cobalt ion for comparison. XRD patterns indicated that the cobalt powder obtained under these electrodeposition conditions consisted of only hcp cobalt phase together with tin and copper powder. Changing cobalt ion concentration of electrolyte from 10 g/L to 20 g/L, notable changes in breadths and relative intensities of the peaks were observed as it could be seen from the upper diffraction pattern in Figure 5.20. As it was indicated in the previous microstructure discussions, the quantity of hydrogen evolution was critical for morphology of the powder. Increasing cobalt ion concentration caused decreasing the hydrogen evolution reaction, therefore cobalt powders were formed dendritic in shape with needle-like surface which means defect concentration of the powders were increased. The consequence of the formation of fcc cobalt phase at these

electrodeposition conditions was increased defect concentration (increased microstrain) which could also be derived from significant broadening of the peaks. The remarkable increase in the relative intensity of the (002) peak at 44.76 diffraction angle in the upper diffraction pattern of Figure 5.20 was evidence of the presence of the fcc Co phase through its strongest (111) reflection at the same 2θ angle (JCPDS: 15-0806) [61].

Metallic cobalt has two crystallographic structure, these are fcc and hcp. Around 700 K, low temperature hexagonal closed packed (hcp) structure of Co transforms to a high temperature face-centered cubic (fcc) phase [62]. However, intergrowth of the two phases of cobalt is usual because of small energy difference between two phases [63]. Therefore, detection of both structures in the electrodeposited metallic powder is also in good agreement with the higher defect concentration, since it is known that low transformation energy allowed simultaneous existence of hcp and fcc structures in the bulk cobalt.

CHAPTER 6

CONCLUSION

Recovery of diamond and metal constituents of the valuable particle embedded composite cutting tools were achieved efficiently and comprehensively by means of electrolysis. In addition, more environmentally sensitive method was developed by reducing the amount and concentration of acid in already existing recycling applications of valuable particle embedded composite cutting tools.

In electrochemical cell, diamond particles were easily gathered which were collected from the bottom of electrolyte after dissolution of discarded cutting tools by application of current.

The current density values that were applied for recovery of diamond embedded bronze cutting tools could not be high enough for reduction of tin at the cathode. Therefore, tin powders were also collected from the bottom of the electrolyte and filtered after the experiments like diamond particles.

For bronze matrix diamond embedded composite cutting tools, current density, temperature, acid and CuSO_4 concentration of electrolyte were important parameters and these were optimized to obtain compact, dense copper powders having small surface area to mass ratio and having reasonable particle size.

Among all parameters, 8.37 A/dm^2 current density, 40°C temperature, $0.5 \text{ M H}_2\text{SO}_4$ concentration and 15 g/L copper ion concentration were optimum values to obtain compact, dense powder with minimum surface area and average particle size that provides good sinterability and flowability.

For recovery of metallic constituents of diamond embedded cutting tools having cobalt-copper-tin matrix, 70 A/dm^2 current density, 30°C temperature, $0.5 \text{ M H}_2\text{SO}_4$

concentration, 10 g/L Co^{2+} concentration were optimum values to have dense, agglomerated cobalt powders, copper powder with less branched dendritic structure and uniform, regular tin powders having small surface area to mass ratio and having reasonable particle size.

Hydrogen evolution reaction was important side reaction in metal electrodeposition processes that affected morphology and properties of all deposited metallic powders. Therefore, optimization of electrodeposition parameters of metallic powders requires optimized hydrogen formation reaction.

REFERENCES

- [1] L. Wang, G. Zhang, and F. Ma, "A study on comprehensive recycling of waste diamond tools," *Rare Met.*, vol. 31, no. 1, pp. 88–91, 2012.
- [2] M. Filgueira and D. G. Pinatti, "Processing of Diamond Composites for Cutting Tools by Powder Metallurgy and Rotary Forging," *Mater. Sci. Forum*, vol. 416–418, no. 1, pp. 228–234, 2003.
- [3] C. Browning, "Circular diamond saw blade incorporating a novel cutting segment," US Patent Number 4,739,745, 1988.
- [4] K. . Öksüz and M. Şimşir, "Processing and Mechanical Properties of B₄C/Diamond Impregnated Fe/Co MMC," *Acta Phys. Pol. A*, vol. 127, no. 4, pp. 1139–1141, 2015.
- [5] J. Konstanty, "Powder Metallurgy Diamond Tools – A Review of Manufacturing Routes," *Mater. Sci. Forum*, vol. 534–536, no. January 2007, pp. 1121–1124, 2007.
- [6] Y. S. Liao and S. Y. Luo, "Effects of matrix characteristics on diamond composites," *J. Mater. Sci.*, vol. 28, no. 5, pp. 1245–1251, 1993.
- [7] "Global Synthetic Diamond Market - Trends and Forecasts (2016-2021)," *Research and Markets*. [Online]. Available: <https://www.businesswire.com/news/home/20171030005490/en/Global-Synthetic-Diamond-Market-Report-2017-->.
- [8] P. Zimmisky, "How High Quality Synthetic Diamonds Will Impact the Market."
- [9] E. Norland, "Copper: Supply and Demand Dynamics," *CME Group*. [Online]. Available: <http://www.cmegroup.com/education/featured-reports/copper-supply-and-demand-dynamics.html>.
- [10] "Distribution of cobalt demand worldwide as of 2016, by industry," *The Statistics Portal, Statista*. [Online]. Available: <https://www.statista.com/statistics/655947/global-cobalt-demand-distribution-by-industry/>. [Accessed: 22-Apr-2018].
- [11] F. Imre-Lucaci, "Electrochemical methods for recovery of copper from waste waters and solid wastes_PhD Thesis," "Babe,s-Bolyai" University Cluj–Napoca.
- [12] C. Study, "Prüfung und Aktualisierung von Rohstoffparametern_Future availability & supplies," 2016.
- [13] O. Celep, G. Aydin, and I. Karakurt, "Diamond recovery from waste sawblades:

- A preliminary investigation,” *J. Eng. Manuf.*, vol. Part B, 2013.
- [14] R. M. German, *Powder metallurgy science*, 2nd ed. Princeton, N.J. : Metal Powder Industries Federation, 1994.
- [15] M. G. Pavlovic and K. I. Popov, “Metal Powder Production by Electrolysis,” *Electrochemistry Encyclopedia*. .
- [16] G. Orhan and G. Hapçı, “Effect of electrolysis parameters on the morphologies of copper powder obtained in a rotating cylinder electrode cell,” vol. 201, no. 1, pp. 57–63.
- [17] N. Ibl and K. Schadegg, “Surface Roughness Effects in the Electrodeposition of Copper in the Limiting Current Range,” *J. Electrochem. Soc.*, vol. 114, no. 1, pp. 54–58, 1967.
- [18] G. Wranglen, *Electrodeposition of Metal Powders*, vol. 97, no. 11. Oxford, United Kingdom: Elsevier Science Ltd, 1950.
- [19] K. I. Popov, M. D. Maksimović, J. D. Trnjančev, and M. G. Pavlović, “Dendritic electrocrystallization and the mechanism of powder formation in the potentiostatic electrodeposition of metals,” *J. Appl. Electrochem.*, vol. 11, no. 2, pp. 239–246.
- [20] J. L. Barton and J. O. Bockris, “The Electrolytic Growth of Dendrites from Ionic Solutions,” *Proc. R. Soc. Lond. A. Math. Phys. Sci.*, vol. 268, no. 1335, pp. 485–505.
- [21] M. D. Maksimović, K. I. Popov, and M. G. Pavlović, “Mechanism of Electrode Surface Roughening in Galvanostatic Metal Deposition on A Rotating Disc Electrode,” *Bull. la Société Chim. Beogr.*, vol. 44, pp. 687–693, 1979.
- [22] M. D. Maksimović, K. I. Popov, L. J. Jovic’, and M. G. Pavlović, “Mechanism of Electrode Surface Roughening in Galvanostatic Metal Deposition at Natural Convection,” *Bull. la Société Chim. Beogr.*, vol. 44, pp. 547–554, 1979.
- [23] A. R. DespićK. and I. Popov, “Transport-Controlled Deposition and Dissolution of Metals,” in *Modern Aspects of Electrochemistry No. 7*, Springer, Boston, MA, 1972, pp. 199–313.
- [24] K. I. Popov, N. D. Nikolić, and L. Rakočević Zlatko, “An estimation of the interfacial energy of the copper-copper sulphate solution interface and of the specific surface of copper powder,” *J. Serbian Chem. Soc.*, vol. 67, pp. 635–638, 2002.
- [25] C. Paper, E. Akbarzadeh, U. Polit, and E. Akbarzadeh, “Particle shape and size modification and related property improvements for industrial copper powder,” no. August 2010, 2014.
- [26] K. I. Popov, M. G. Pavlović, M. D. Maksimović, and S. S. Krstajić, “The

- comparison of galvanostatic and potentiostatic copper powder deposition on platinum and aluminium electrodes,” *J. Appl. Electrochem.*, vol. 8, no. 6, pp. 503–514, 1978.
- [27] A. Calusaru, *Electrodeposition of Metal Powders (Materials Science Monographs)*. Elsevier Science Ltd, New York, 1979.
- [28] S. S. Djokić, Ed., “Electrochemical Production of Metal Powders,” in *Modern Aspects of Electrochemistry*, 54th ed., Springer US.
- [29] K. I. Popov, N. V. Krstajic, and M. I. Cekerevac, “The mechanism of formation of coarse and disperse electrodeposits,” *Mod. Asp. Electrochem.*, vol. 30, pp. 261–311.
- [30] M. Rosso, E. Chassaing, V. Fleury, and J.-N. Chazalviel, “Shape evolution of metals electrodeposited from binary electrolytes,” *J. Electroanal. Chem.*, vol. 559, pp. 165–173, 2003.
- [31] N. D. Nikolić, L. J. Pavlović, M. G. Pavlović, and K. I. Popov, “Morphologies of electrochemically formed copper powder particles and their dependence on the quantity of evolved hydrogen,” *Powder Technol.*, vol. 185, no. 3, pp. 195–201, 2008.
- [32] J. Konstanty, *Powder Metallurgy Diamond Tools*. 2005.
- [33] H. Xian, Gu. Xue, L. Ping, H. Kai, and X. Kai, “Recovery of Nickel, Cobalt and Manganese from Waste Acid Solution from Synthesis of Artificial Diamond,” *Hydrometall. China*, no. 03, 2005.
- [34] M. Erg, “Recovery of Metals From Solutions Obtained by Cutting Tool Recycling,” pp. 355–358, 2016.
- [35] “COMSOL Multiphysics, Version 5.2.” [Online]. Available: www.comsol.com.
- [36] S. Jiang and J. H. ter Horst, “Crystal Nucleation Rates from Probability Distributions of Induction Times,” *Cryst. Growth&Design*, vol. 11, no. 1, pp. 256–261, 2011.
- [37] H. Frydrych, A. Romanski, and J. Konstanty, “The influence of iron content and powder metallurgy processing route on microstructure and mechanical properties of cobalt-iron materials,” *Arch. Metall. Mater.*, vol. 49, no. 4, pp. 973–980, 2004.
- [38] S. Lowell and J. E. Shields, *Powder Surface Area and Porosity*, 2nd Editio. London New York: Chapman and Hall Ltd., 1984.
- [39] M. G. Pavlović, L. J. Pavlović, V. M. Maksimović, N. D. Nikolićand, and K. I. Popov, “Characterization and morphology of copper powder particles as a function of different electrolytic regimes,” *Int. J. Electrochem. Sci.*, vol. 5, no.

- 12, pp. 1862–1878, 2010.
- [40] K. Popov, B. Grgur, and S. S. Djokić, *Fundamental Aspects of Electrometallurgy*, 1st ed. New York, USA: Springer US, 2002.
- [41] N. D. Nikolić, K. I. Popov, L. J. Pavlović, and M. . Pavlović, “Morphologies of copper deposits obtained by the electrodeposition at high overpotentials,” *Surf. Coat. Technol.*, vol. 201, pp. 560–566, 2006.
- [42] T. J. O’Keefe, “Techniques for evaluating electrolytes for metal recovery,” *J. Electroanal. Chem. Interfacial Electrochem.*, vol. 168, no. 1–2, pp. 131–146.
- [43] J.-L. Delplancke, M. Sun, T. J. O’Keefe, and R. Winand, “Nucleation of electrodeposited copper on anodized titanium,” *Hydrometallurgy*, vol. 23, no. 1, pp. 47–66.
- [44] E. Y. Yazici and H. Deveci, “Extraction of metals from waste printed circuit boards (WPCBs) in H₂SO₄–CuSO₄–NaCl solutions,” *Hydrometallurgy*, vol. 139, pp. 30–38.
- [45] W. He, X. Duan, and L. Zhu, “Characterization of ultrafine copper powder prepared by novel electrodeposition method,” *J. Cent. South Univ. Technol.*
- [46] G. Orhan and G. Hapçı, “Effect of electrolysis parameters on the morphologies of copper powder obtained in a rotating cylinder electrode cell,” *Powder Technol.*, vol. 201, no. 1, pp. 57–63.
- [47] K. I. Popov and M. G. Pavlović, “Electrodeposition of Metal Powders with Controlled Particle Grain Size and Morphology,” *Mod. Asp. Electrochem.*, vol. 24, pp. 299–391, 1993.
- [48] N. D. Nikolic, K. I. Popov, L. J. Pavlovic, and M. G. Pavlovic, “Determination of Critical Conditions for the Formation of Electrodeposited Copper Structures Suitable for Electrodes in Electrochemical Devices,” *Sensors*, vol. 7, no. 1, pp. 1–15, 2007.
- [49] N. S. Randhawa, D. C. Sau, and M. Kumar, “Direct electrolytic refining of end-of-life industrial copper waste scraps for production of high purity copper powder,” *Russ. J. Non-Ferrous Met.*, vol. 57, no. 4, pp. 367–373, 2016.
- [50] S. A. Amadi, D. R. Gabe, and M. Goodenough, “An electrochemical mass transport sensor to study agitation in electroplating processes,” *J. Appl. Electrochem.*, vol. 21, no. 12, pp. 1114–1119.
- [51] N. D. Nikolić, K. I. Popov, L. J. Pavlović, and M. G. Pavlović, “The effect of hydrogen codeposition on the morphology of copper electrodeposits. I. the concept of effective overpotential,” *J. Electroanal. Chem.*, vol. 588, no. 1, pp. 88–98, 2006.
- [52] S. S. Naboychenko, I. B. Murashova, and O. D. Neikov, “Production of Copper

- and Copper Alloy Powders,” in *Handbook of Non-Ferrous Metal Powders*, 2nd Editio., Oxford: Elsevier, 2009, pp. 331–368.
- [53] N. D. Nikolić, L. J. Pavlović, M. G. Pavlović, and K. I. Popov, “Morphologies of electrochemically formed copper powder particles and their dependence on the quantity of evolved hydrogen,” *Powder Technol.*, vol. 185, no. 3, pp. 195–201.
- [54] N. D. Nikolić and K. I. Popov, “Hydrogen Co-deposition Effects on the Structure of Electrodeposited Copper,” in *Modern Aspects of Electrochemistry*, vol. 48, S. Djokic, Ed. Springer, New York, NY, 2010, pp. 1–70.
- [55] “General, Atomic and Crystallographic Properties and Features of Copper,” *Copper Development Association Inc.* .
- [56] Collaboration: Authors and editors of the volumes III/17E-17F-41C, “Cuprous oxide (Cu₂O) crystal structure, lattice parameters,” *Non-Tetrahedrally Bond. Elem. Bin. Compd. I*, vol. 41C, pp. 1–3.
- [57] N. D. Nikolić and K. I. Popov, “Electrodeposition: Theory and Practice,” in *Modern Aspects of Electrochemistry*, S. S. Djokić, Ed. Berlin: Springer, 2010, p. 1.
- [58] N. D. Nikolić, G. Branković, and M. G. Pavlović, *Powder Technology*. 2012.
- [59] M. Engineers and S. A. Scientific, “International Conference Processing and Structure of Materials held on Palic, Serbia May 27- 29, 2010,” 2010.
- [60] R. W. G. WYCKOFF, *Crystal Structures*, Second Edi., vol. 1. New York: Interscience Publishers, New York, New York Hexagonal closest packed, hcp, structure, 1963.
- [61] J. Häglund, A. Fernández Guillermet, G. Grimvall, and M. Körling, “Theory of bonding in transition-metal carbides and nitrides,” *Phys. Rev. B* 48, 1993.
- [62] T. Nishizawa and K. Ishida, “The Co (Cobalt) system,” *Bull. Alloy Phase Diagrams*, vol. 4, no. 4, pp. 387–390.
- [63] B. Lee, R. Alsenz, A. Ignatiev, M. Van Hove, and M. A. Van Hove, “Surface structures of the two allotropic phases of cobalt,” *Phys. Rev. B*. 17, no. 4, pp. 1510–1520, 1978.

